AD-A031 496 NORTHEASTERN UNIV BOSTON MASS DEPT OF ELECTRICAL EN--ETC F/G 4/1
NUCLEAR BURST INDUCED SHOCK WAVE MODELLING OF ENERGETIC ELECTRO--ETC(U)
JUL 76 J W CIPOLLA, K I GOLDEN, A L PAVEL F19628-75-C-0012
UNCLASSIFIED AFGL-TR-76-0186 NL

1 OF 1
ADA031496

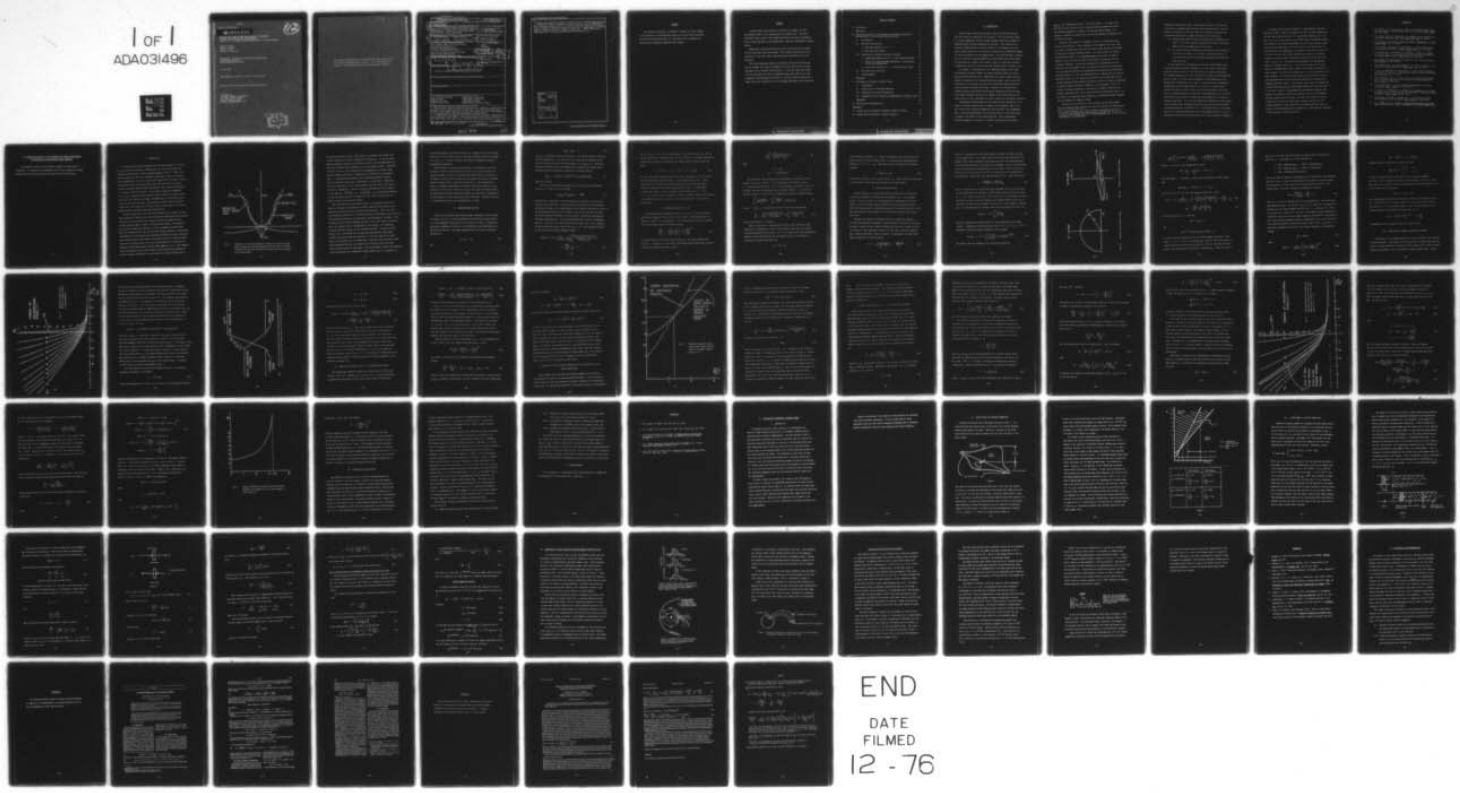

END

DATE
FILMED
12 - 76

AFGL-TR-76-0186

NUCLEAR BURST INDUCED SHOCK WAVE MODELLING OF ENERGETIC ELECTRON INJECTION INTO THE MAGNETOSPHERE: Application of streaming plasma instabilities to shock structures.

John W. Cipolla
Kenneth I. Golden
Arthur L. Pavel
Michael B. Silevitch

Departments of Mechanical and Electrical Engineering
Northeastern University
Boston, Massachusetts 02115

31 July 1976

FINAL REPORT for period 1 July 1974 - 30 June 1976

Approved for public release; distribution unlimited.

Prepared for:
AIR FORCE GEOPHYSICS LABORATORY
AIR FORCE SYSTEMS COMMAND
UNITED STATES AIR FORCE
BEDFORD, MASSACHUSETTS 01730

Qualified requestors may obtain additional copies from the Defense Documentation Center. All others should apply to the National Technical Information Service

Unclassified

SECURITY CLASSIFICATION OF THIS PAGE (When Data Entered)

REPORT DOCUMENTATION PAGE

READ INSTRUCTIONS BEFORE COMPLETING FORM

1. REPORT NUMBER: AFGL-TR-76-0186	2. GOVT ACCESSION NO. / 3. RECIPIENT'S CATALOG NUMBER
4. TITLE (and Subtitle): Nuclear Burst Induced Shock Wave Modelling of Energetic Electron Injection into the Magnetosphere: Application of streaming plasma instabilities to shock structures.	5. TYPE OF REPORT & PERIOD COVERED: 1 July 1974-30 June 1976 Final Report 6. PERFORMING ORG. REPORT NUMBER
7. AUTHOR(s): John W. Cipolla, Arthur L. Pavel, Kenneth I. Golden, Michael B. Silevitch	8. CONTRACT OR GRANT NUMBER(s): F19628-75-C-0012
9. PERFORMING ORGANIZATION NAME AND ADDRESS: K.I. Golden, Dept. of Electrical Eng'g. Northeastern University Boston, Massachusetts 02115	10. PROGRAM ELEMENT, PROJECT, TASK AREA & WORK UNIT NUMBERS: 61102F 8600-06-03
11. CONTROLLING OFFICE NAME AND ADDRESS: Air Force Geophysics Laboratory (PHE) Hanscom AFB, Massachusetts Monitor/PHE/Capt. Arthur L. Pavel	12. REPORT DATE: 31 July 1976 13. NUMBER OF PAGES: 77
14. MONITORING AGENCY NAME & ADDRESS (if different from Controlling Office): Final Rept. 1 Jul 74-30 Jun 76	15. SECURITY CLASS. (of this report): Unclassified 15a. DECLASSIFICATION/DOWNGRADING SCHEDULE

16. DISTRIBUTION STATEMENT (of this Report)

Approved for public release; distribution unlimited.

17. DISTRIBUTION STATEMENT (of the abstract entered in Block 20, if different from Report)

18. SUPPLEMENTARY NOTES

19. KEY WORDS (Continue on reverse side if necessary and identify by block number)

ion cyclotron beam mode	perpendicular shock wave
whistler mode	beam-plasma instability
magnetosonic mode	spacecraft charging
parallel shock wave	magnetospheric electron fluxes

20. ABSTRACT (Continue on reverse side if necessary and identify by block number)

A parallel shock wave structure is modelled as a region of interpenetrating streams of cold unshocked and hot shocked ions. Our liner dispersion theory predicts that unstable whistlers can stand and therefore grow to large amplitude at the leading edge of weak and intermediate strength shocks.

Magnetosonic instabilities and their role in the structure of perpendicular shock waves were also studied. Since these instabilities are not stationary in the shock layer, they cannot play a principal role in the structure. → next page -over-

DD FORM 1 JAN 73 1473 EDITION OF 1 NOV 65 IS OBSOLETE

Unclassified

SECURITY CLASSIFICATION OF THIS PAGE (When Data Entered)

400 914

cont

→ The linear dispersion analysis of parallel shock structures has been used to estimate the fluxes of energetic electrons injected into the magnetosphere due to multiple nuclear bursts. It has been found that fluxes of 20 kev electrons two orders of magnitude larger than those due to magnetospheric substorms might be expected to occur for times as long as 30 s. These could play a significant role in charging synchronous orbit spacecraft. ↑

PREFACE

The authors are grateful to Professor G. Kalman for useful comments on the structure of the dispersion relation for ion cyclotron beam mode-whistler mode interactions and to D. Chiaverini and A. Voyatzakis for assistance with numerical computation and figures.

SUMMARY

A parallel shock wave structure is modelled as a region of interpenetrating streams of cold unshocked and hot shocked ions. Our linear dispersion theory predicts that unstable whistlers can stand and therefore grow to large amplitude at the leading edge of weak and intermediate strength shocks.

Magnetosonic instabilities and their role in the structure of perpendicular shock waves were also studied. Since these instabilities are not stationary in the shock layer, they cannot play a principal role in the structure.

The linear dispersion analysis of parallel shock structures has been used to estimate the fluxes of energetic electrons injected into the magnetosphere due to multiple nuclear bursts. It has been found that fluxes of 20 kev electrons two orders of magnitude larger than those due to magnetospheric substorms might be expected to occur for times as long as 30 s. These could play a significant role in charging synchronous orbit spacecraft.

TABLE OF CONTENTS

A. INTRODUCTION

During a high altitude nuclear burst, debris particles are ejected from the fireball by essentially two processes. The first process, which is collision dominated, involves charge exchange interactions between the expanding debris ions and background air neutrals. This results in the ejection of debris neutrals from the fireball; it is unlikely that this neutral debris ejection can be directly connected with any mechanism leading to electron injection into the magnetosphere. The second process, collisionless in nature and involving turbulent coupling between the ejected debris and background air plasmas, does, however, appear to bring about electron streaming into the Van Allen belts and has therefore been of interest to us.

For example, in the presence of the compressed magnetic field which can penetrate the debris bubble, the plasma turbulence takes the form of large amplitude whistler waves. These waves can suitably couple the background air plasma with the expanding debris-air plasma. More and more hot electrons are thus acquired and some have sufficiently large velocities to escape along the distended field lines. Moreover, the nonlinear wave-resonant particle interactions should produce anomalous resistivity whose scale length determines the extent of magnetic field penetration into the bubble which, in turn, determines the rate of escape of β and plasma electrons.

Superalfvénic debris plasma can also escape directly through loss cone exits in the debris bubble since, in general, the cylindrical axis of the bomb casing is not initially aligned with the direction of the geomagnetic field. The more perpendicular the cylindrical axis is to the field lines, the greater the number of such escape particles. Their superalfvénic velocities suggest the formation of parallel collisionless shock waves

($V_{shock} \parallel B$ = geomagnetic field). Our studies (Refs. 1, 2) reveal that such shock fronts are structured by turbulent whistler modes which couple the incoming background air plasma to the shocked debris plasma. Air plasma can therefore be picked up by the loss cone debris and deposited into the Van Allen belts.

Evidently, the presence of a magnetic field has a significant effect on shock wave structure. First, gradients in the magnetic field give rise to electron currents that can drive ion acoustic waves unstable and increase the effective collision frequency (Refs. 3, 4) (this should also dictate the penetration depth of the compressed magnetic field into the debris bubble, so that the rate of escape of debris and air electrons could be profoundly affected). Second, when propagation is perpendicular to the magnetic field, the magnetic field can inhibit the electrons from shorting out ion plasma oscillations for wavelengths long compared with the electron gyroradius (Refs. 5 to 10); for wavelengths short compared with the electron gyroradius (Refs. 11, 12), interactions between the ion beam mode and the electron Bernstein modes generate instabilities which are, however, stabilized by electron heating, resonance broadening, or ion trapping. Third, for oblique or parallel propagation, interactions of whistler waves with ion acoustic beam modes (Ref. 13)* or with ion-cyclotron beam modes (Refs. 1, 2) are likely to be important and the existence of whistlers assuredly depends upon the presence of a magnetic field.

During the two year period of this contract, we have investigated several streaming plasma instabilities and their roles in the structures of

*The s called "modified" two stream instability described in Refs. 7 to 9 is operative for propagation angles slightly less than 90°, so that it is actually the limiting form of the Lindman-Drummond (Ref. 13) ion acoustic beam-whistler type instability.

collisionless perpendicular (Ref. 10) and parallel (Ref. 2) shock waves formed ahead of expanding high altitude nuclear debris pistons. The following two instabilities have been found to be especially attractive as collisionless mechanisms for pickup and heating of air electrons:

(i) Current-driven modified two-stream instability of McBride et al (Refs. 7 to 9) which should be operative over most of the debris bubble surface excluding the loss cone exits.

(ii) Ion cyclotron beam mode-whistler mode (current-free) instability of Golden et al (Refs. 1, 2) found to be operative along the field lines and particle trajectories issuing directly from the loss cone exits.

We have modelled the collisionless shock waves as Mott-Smith layers of interpenetrating unshocked (background air) and shocked (thermalized debris-air piston) flows, so that these layers are natural environments for streaming instabilities. Our investigations (based on linear dispersion theory, see Ref. 10) reveal that the magnetic counterstreaming ion-ion instability of Papadopoulos et al (Ref. 5) cannot structure collisionless perpendicular shocks (formed ahead of the portion of the bubble which excludes the loss cone exits) since, in the reference frame of the shock front, the ensuing magnetosonic modes are blown downstream out of the shock layer before they can grow to sufficiently large amplitude to scatter incoming air particles. It is far more likely that perpendicular shock layers are structured by the turbulence arising from the current-driven modified two-stream instability of McBride et al. A published reprint of our recent work on the crossfield magnetosonic two-stream instability and its role in perpendicular shock wave structures (Ref. 10) is also included in Appendix A.

Our recent linear dispersion theoretic investigations of parallel shock layers (Ref. 2) which form ahead of the debris plasma issuing from the loss cone exits reveal that, for a given Mach number $M_A > M^* = 2.77$ ($M_A = V_u/C_A$, V_u = shock velocity, C_A = Alfvén speed in unshocked plasma), the shocked hot ion cyclotron beam mode can always drive unstable a particular whistler mode which, in the rest frame of the shock front, is stationary near the leading edge. An analysis of the shock interior reveals that the shock Mach number determines the portion of the shock thickness in which unstable whistlers are stationary in the shock rest frame. For $M_A = 2.77$, such modes may stand only at the leading edge, whereas for stronger shocks ($M_A > 2.77$), they may stand at all points between the leading edge and some interior point which is dependent on shock strength. For very strong shocks ($M_A \gg 1$), fully one-third of the shock thickness is filled with these modes, which can therefore grow to large amplitude and couple the quiescent background air plasma to the expanding debris-air piston. In an earlier study, where the shocked ion cyclotron beam mode was less realistically modelled as cold fluid (Ref. 1), M^* was found to equal 5.5 suggesting that the turbulent whistler mode mechanism for momentum coupling was operative only in the intermediate strength parallel shock structures. Our new theory based on the more realistic hot ion cyclotron beam model, however, predicts that this coupling mechanism is also operative in the weaker parallel shocks encountered in high altitude nuclear explosions. A more detailed discussion of this analysis is presented in Sec. B.

REFERENCES

1. K.I. Golden, L.M. Linson, and S.A. Mani, Ion Streaming Instabilities with Application to Collisionless Shock Wave Structure, Phys. Fluids 16, 2319 (1973).

2. J.W. Cipolla and K.I. Golden, Role of Streaming Plasma Instabilities in Parallel Shock Wave Structures, Phys. Lett. 51A, 251 (1975).

3. J.D. Jackson, Longitudinal Plasma Oscillations, Plasma Phys. (J. Nucl. Energy, Part C) 1, 171 (1960).

4. T.E. Stringer, Electrostatic Instabilities in Current-Carrying and Counterstreaming Plasmas, J. Nucl. Energy, Part C, 6, 267 (1964).

5. K. Papadopoulos, R.C. Davidson, J.M. Dawson, I. Haber, D.A. Hammer, N.A. Krall, and R. Shanny, Heating of Counterstreaming Ion Beams in an External Magnetic Field, Phys. Fluids 14, 849 (1971).

6. R.W. Landau, Counterstreaming Ion Instability for Arbitrary Angles, Phys. Fluids 15, 1991 (1972).

7. J.B. McBride and E. Ott, Electromagnetic and Finite β_e Effects on the Modified Two Stream Instability, Phys. Lett. 39A, 363 (1972).

8. E. Ott, J.B. McBride, J.H. Orens, and J.P. Boris, Turbulent Heating in Computer Simulations of the Modified Plasma Two Stream Instability, Phys. Rev. Lett. 28, 88 (1972).

9. J.B. McBride, E. Ott, J.P. Boris, and J.H. Orens, Theory and Simulation of Turbulent Heating by the Modified Two Stream Instability, Phys. Fluids 15, 2367 (1972).

10. J.W. Cipolla and K.I. Golden, Crossfield Magnetosonic Two Stream Instability, Can. J. Phys. 53, 1022 (1975).

11. M. Lampe, W.M. Mannheimer, J.B. McBride, K. Papadopoulos, J.H. Orens, R. Shanny, and R.N. Sudan, Theory and Simulation of the Beam Cyclotron Instability, Phys. Fluids 15, 662 (1972).

12. D. Forslund, R. Morse, C. Nielson, and J. Fu, Electron Cyclotron Drift Instability and Turbulence, Phys. Fluids 15, 1303 (1972).

13. E.L. Lindmand and W.E. Drummond, Studies of Oblique Shock Structure, Report ARA-28, Austin Research Associates, Inc., Austin, Texas, 1971).

B. THEORETICAL ANALYSIS OF LOW FREQUENCY TWO STREAM INSTABILITIES AND THEIR ROLE IN COLLISIONLESS SHOCK STRUCTURE

The material in this section comprises a manuscript submitted for publication. It summarizes our theoretical work on low frequency two stream instabilities and their application to parallel shock wave structure.

I. INTRODUCTION

It has been theoretically demonstrated that low frequency ($\omega \sim 1\text{-}5\ \Omega_{ci}$, Ω_{ci} = ion cyclotron frequency) instabilities can arise from relative ion streaming motions along a constant applied magnetic field.[1,2] These were first analyzed by Kovner[1] who considered, among other current-free initial flow configurations, one where (in the rest frame of the electrons) a tenuous ion beam penetrates a relatively dense ion plasma; here the tenuous ion cyclotron beam mode interacts with well-defined right circularly polarized ion cyclotron and whistler modes. For the case of parallel propagation ($\underset{\sim}{k} \parallel \underset{\sim}{B}_o$, $\underset{\sim}{B}_o$ = constant applied magnetic field) through cold plasma, Kovner showed that only the whistler modes (corresponding to interactions B and C in Fig. 1) can become unstable. More recently, Golden, Linson, and Mani[2] extended the cold plasma part of Kovner's work to take account of ion beams having densities comparable with the plasma density.

The most significant result reported by Golden et al, however, is that these unstable ion beam-whistler wave interactions could produce the turbulent structure of parallel shock waves (shock waves which propagate along a constant applied magnetic field) in collisionless plasma. By solving the $\underset{\sim}{k} \parallel \underset{\sim}{B}_o$ linear dispersion relation at points throughout the shock layer under the assumption that the local ion distribution function is a Mott-Smith superposition of interpenetrating unshocked and shocked ion flows (electrons were treated simply as warm fluid), the authors found that certain unstable modes near the leading edge of the shock could propagate at precisely the velocity of the leading edge for Alfvén Mach numbers $M_A \geq 5.5$. This suggests that such modes have ample time to grow to sufficiently large amplitude to scatter incoming (unshocked) ions and create the required dissipation for

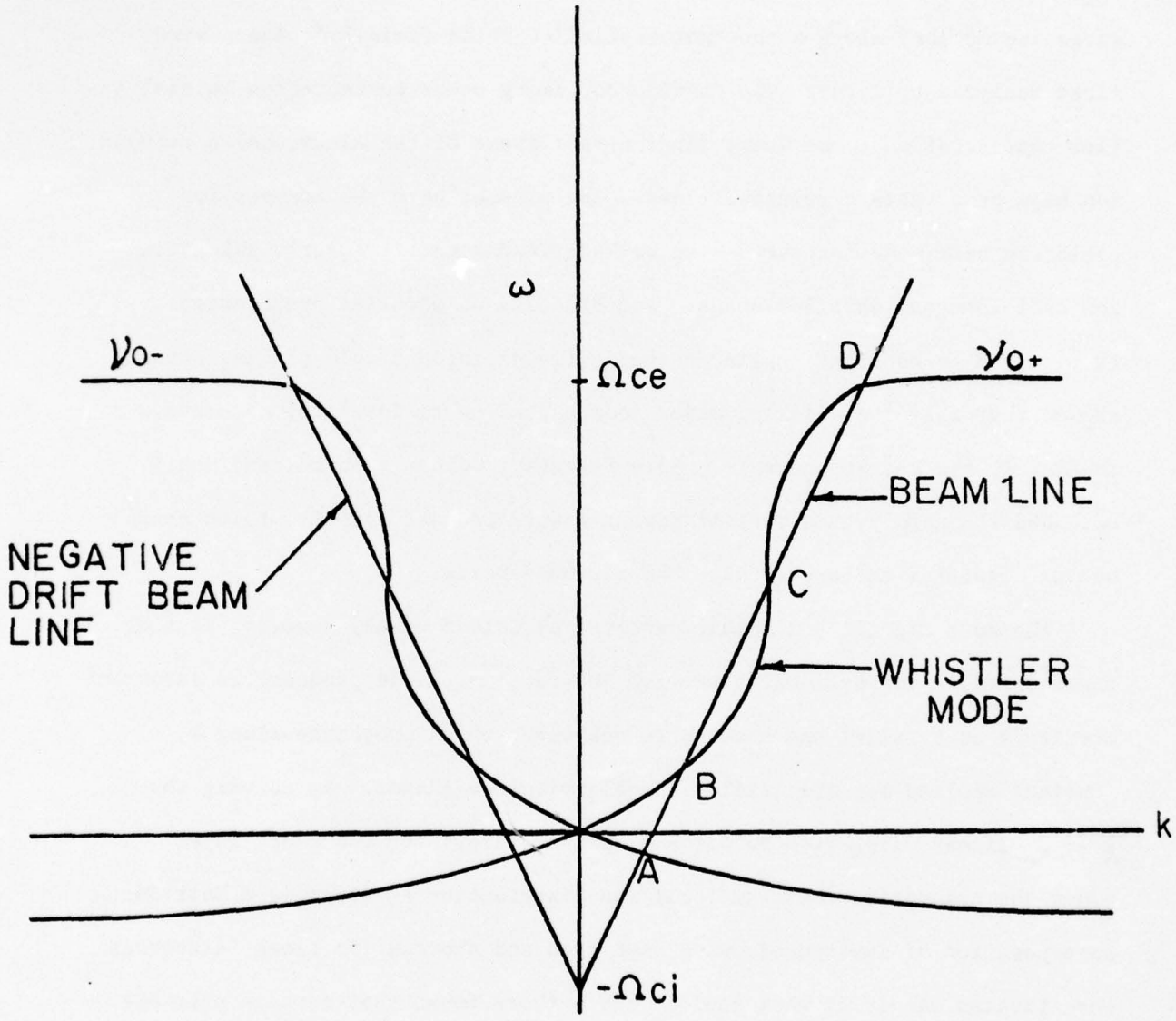

Fig. 1 Schematic of the linear dispersion relation for parallel propagation showing the possible interaction of the right circularly polarized ion cyclotron and whistler branches with the drifting ion cyclotron mode.

intermediate strength shocks. Their theory has, however, two serious limitations imposed for the sake of mathematical simplicity: (i) only unstable modes propagating along $\underset{\sim}{B}_o$ were considered and (ii) the interpenetrating ion flows were unrealistically modelled as cold monoenergetic beams. Concerning the first of these, if one considers waves propagating at an angle to $\underset{\sim}{B}_o$, electron thermal effects have a significant interaction with the magnetic modes. A discussion and analysis of the resulting dispersion relation, which is much more complicated, is deferred to a later paper. Concerning the second limitation, it is at once apparent that the shocked ions are, by definition, thermalized. Moreover, even the unshocked ions must be sufficiently warm ($C_S = \sqrt{5\kappa T/3m_i} > C_A = B_o/\sqrt{4\pi m_i n_u}$, n_u = unshocked ion density) to preclude the possibility of "switch-on" type shocks[3] (rotation of the magnetic field across the shock layers).

The main objective of the present paper is to re-examine the role of these ion streaming instabilities in parallel shock wave structures by more realistically taking account of the ion thermal effects. This we do first by allowing the shocked ions to be Maxwellian with final density, mean velocity, and temperature dictated by the gas-dynamic Rankine-Hugoniot relations. Then following the Mott-Smith formalism, the ions, in the rest frame of the shock front, are modelled as the superposition of two streams: hot downstream particles drifting through the cold upstream particles. We shall see that for $M_A \gtrsim 2.77$, the shocked hot ion cyclotron beam mode can always drive unstable a particular whistler mode which, in the rest frame of the shock front, is stationary near the leading edge. Moreover, such stationary growth modes apparently exist up to one-third of the distance across the shock layer starting from the leading edge. Thus the turbulent whistler mode momentum coupling mechanism for intermediate strength shocks ($M_A \gtrsim 5.5$) suggested by

the previous cold ion cyclotron beam theory is suggested as well by the hot beam theory of the present paper for the weaker parallel shocks in the range $2.77 \leq M_A \leq 5.5$. Finally we discuss the effects of relaxing the cold upstream plasma assumption.

Before going into the shock wave problem, it is instructive to first analyze the linear dispersion relation in the initial (current-free) configuration where the warm electrons have zero mean velocity, and where the hot beam ions counterstream through the cold plasma ions along the constant external magnetic field. This we do in Section II. The application of these ion streaming instabilities to parallel shock wave structure is then carried out in Section III where now, in the rest frame of the shock front, the mean motion of the warm electron fluid in the shock layer is governed by the requirements of local charge and current neutrality. Finally in Section IV, conclusions are drawn and recommendations are made.

II. ELECTRON FRAME ANALYSIS

Consider an unbounded collisionless plasma consisting of two ion beams of densities n_1 and n_2 counterstreaming with velocities $\underset{\sim}{V}_1$ and $\underset{\sim}{V}_2$ parallel to a steady magnetic field $\underset{\sim}{B}_o$ taken to lie along the z axis. We assume the unperturbed background electrons to be described by a zero mean Maxwellian distribution function. The charge neutrality and zero current conditions are given by

$$n_1 + n_2 = n_e \tag{1}$$

and

$$n_1 \underset{\sim}{V}_1 + n_2 \underset{\sim}{V}_2 = 0 \tag{2}$$

where n_e is the number density of electrons. For the low frequency case that we are interested in, it is crucial that the zero current condition (2) be met for arbitrary values of the beam strength ($0 \leq n_2/n_e \leq 1$). Deviations from the unperturbed state are assumed to be governed by the linear Vlasov equation with an unperturbed ion distribution function given by

$$f_i(\underset{\sim}{v}) = n_1 \delta(\underset{\sim}{v}-\underset{\sim}{V}_1) + n_2(\pi c_2^2)^{-3/2} \exp\left[-(\underset{\sim}{v}-\underset{\sim}{V}_2)^2/c_2^2\right] \tag{3}$$

where $c_2^2 = 2\kappa T_2/m_i$.

For the case of parallel propagation ($\underset{\sim}{k} \,||\, \underset{\sim}{B}_o$) the linear dispersion relation is, in the electron rest frame,

$$\varepsilon_{xx}(\underset{\sim}{k},\omega) \pm i\varepsilon_{xy}(\underset{\sim}{k},\omega) = \left(\frac{kc}{\omega}\right)^2. \tag{4}$$

The dielectric components in (4) are calculated by addition of the ion and electron polarizabilities. These well known polarizabilities are formulated explicitly in terms of the (unperturbed) ion and electron distribution functions and therefore take account of the bimodal nature of the ions [Eq. (3)] and the locally Maxwellian behavior of the electrons. We make the following low frequency approximations: (i) the vacuum displacement current is negligibly small ($\omega << kc$), and (ii) the electrons have zero mass ($|\omega| << \Omega_{ce} = eB_o/m_e c$) so they can be modelled as a warm fluid ($kr_{Le} << 1$). The dispersion relation in the electron rest frame ultimately becomes

$$D(k,\omega) = (1-\eta)\frac{\Omega_{ci}}{\omega - kV_1 + \Omega_{ci}} + \frac{\eta}{\sqrt{\pi}c_2}\int_{-\infty}^{\infty} \frac{(\Omega_{ci}-ku)\exp[-(u/c_2)^2]\,du}{(\omega - kV_2 + \Omega_{ci}) - ku}$$

$$-1 - \frac{k^2 C_A^2}{\Omega_{ci}^2} + \frac{\omega}{\Omega_{ci}} = 0 . \tag{5}$$

Here $\eta = n_2/n_e$ is a measure of beam strength. Note further that k, V_1, and V_2 are the respective z components of $\underset{\sim}{k}$, $\underset{\sim}{V}_1$, and $\underset{\sim}{V}_2$ (and are thus signed quantities). It will also be useful to incorporate the relative drift velocity $\underset{\sim}{U}$ into (5) where

$$U = V_2 - V_1 , \quad V_1 = -\eta U , \quad V_2 = (1-\eta)U \tag{6}$$

and Eqs. (1) and (2) have been used. Note that in the limit $c_2 \to 0$ we recover the cold dispersion relation of Ref. 2. The solution of Eq. (5) $\omega = \omega(k)$ will provide the spectrum of unstable growth modes for current and charge neutral streaming configurations parametrized by η and U. We separately consider the cases of small and arbitrary beam strengths (i.e. $\eta << 1$ or $0 < \eta < 1$), with the weak beam analysis providing a simple check of the arbitrary beam strength calculation, as well as an explicit expression for the linear growth rate.

A. Weak Beam Analysis ($\eta << 1$)

In the weak beam approximation we set $\omega = \nu + i\gamma$, $\gamma << |\nu|$ and perform a perturbation expansion of Eq. (5) for γ and η small. We find that to zeroth order in η there is no contribution to γ but the real part of $D(\omega,k) = 0$ leads to the well known whistler dispersion relation

$$\frac{\nu_o(k)}{\Omega_{ci}} = \frac{k^2C_A^2}{2\Omega_{ci}^2} \pm \frac{kC_A}{\Omega_{ci}}\left[1 + \frac{1}{4}\frac{k^2C_A^2}{\Omega_{ci}^2}\right]^{1/2} . \tag{7}$$

The two branches of this dispersion relation, $\nu_{o\pm}$, are shown schematically in Fig. 1. To obtain the first order contribution to the growth rate, we first rewrite the integral term of Eq. (5) as

$$-\frac{\eta}{\sqrt{\pi}}\int_{-\infty}^{\infty}\frac{e^{-x^2}(\Omega_{ci}/kc_2 - x)}{(x-x_o) - i\gamma/kc_2}\,dx \tag{8}$$

where

$$x = u/c_2$$

$$x_o = (\nu_o - kU + \Omega_{ci})/kc_2 \ .$$

For the initial value problem to be well-defined, the behavior of the integral term in Eq. (8) for $\gamma = 0$ is interpreted as the limit in which $\gamma \to 0$ through positive values. For $\gamma < 0$ the analytic continuation is used by deforming the path of integration into the Landau contour[5]. To account for possible changes in the sign of k, we evaluate (8) using the Plemelj formula

$$\int_{-\infty}^{\infty}\frac{f(x)dx}{(x-x_o) - i\varepsilon} = P\int_{-\infty}^{\infty}\frac{f(x)dx}{x-x_o} + \pi i(\mathrm{sgn}k)f(x_o) \tag{9}$$

(where $\varepsilon = \gamma/kC_2$, $\gamma > 0$) and obtain to first order the growth formula

$$\frac{\gamma}{\Omega_{ci}} = \frac{\sqrt{\pi}\eta}{|k|c_2}\,\frac{(\nu_o+\Omega_{ci})^2(kU-\nu_o)}{\nu_o(\nu_o+2\Omega_{ci})}\,\exp\left[-\frac{(\nu_o-kU+\Omega_{ci})^2}{k^2c_2^2}\right] \tag{10}$$

where we have used $|k| = k(\mathrm{sgn}k)$.

Since our objective in analyzing the electron frame results for this instability is eventually to model a collisionless shock wave, we consider streaming configurations for which $U < 0$. It is clear that strong interactions between the weak warm beam and the cold plasma occur in the vicinity of intersections between the "beam" line

$$\nu_b = kU - \Omega_{ci}$$

and the whistler dispersion ν_o. Since U is negative, the intersections near which growth may occur are shown in Fig. 1 to be with the negative whistler branch (i.e. $k < 0$, $\nu_{o-} > 0$). From (10) we obtain a condition for marginal stability

$$\gamma = 0 \text{ when } \nu_o = kU. \tag{11}$$

Instability, moreover, can occur only for $kU > \nu_o$. These results are discussed in the context of arbitrary beam strengths in the next section.

B. Arbitrary Beam Analysis

In this section, we consider beam-plasma interactions for the general case when the strength of the hot beam is arbitrary (i.e. η is no longer small). This is tantamount to an investigation of growth modes in the interior of a collisionless shock wave modelled as two interpenetrating ion beams with beam strength η parametrizing position in the shock wave (Sec. III). The weak beam-plasma interaction serves to model the leading edge of such a shock wave.

We begin our analysis by observing that for a given beam strength η, the stability-instability boundary is represented by a curve in the U-k space. We derive a family of such curves by finding the region of U-k space in which the solution to the dispersion relation (5), $\omega(k)$, has a positive imaginary part, using the methods of complex analysis. In particular, the well known Nyquist method (5) is based on noting

$$N - P = \frac{1}{2\pi i} \oint_C \frac{D'(\omega)}{D(\omega)}\, d\omega = \frac{[\text{Arg } D]_C}{2\pi} \tag{12}$$

where N - P represents the difference between the number of zeros and poles of the complex function $D(\omega)$ (each counted according to multiplicity) in the region of the ω-plane bounded by the closed contour C. The right-hand side of the equation represents the change in the argument of $D(\omega)$ as C is traversed once in the counterclockwise direction in the ω-plane. We note that $D(\omega)$ is analytic off the real axis, so that if one chooses C to be a semicircle in the upper-half ω-plane (Fig. 2a), then one may set $P = 0$. Thus we may write

$$N = \frac{[\text{Arg } D]_{C_I}}{2\pi} + \frac{[\text{Arg } D]_{C_{II}}}{2\pi} \tag{13}$$

where the contribution to [Arg D] has been separated into the two parts from C_I (the semicircular arc on which $\omega = Re^{i\theta}$) and C_{II} (the real axis for which $-R < \omega < R$), as shown in Fig. 2a. In the limit as $R \to \infty$, C encloses the entire upper-half ω-plane, so that the existence of unstable whistlers will be predicted by the value of N, the number of roots of $D = 0$ with positive imaginary part. We introduce here the analytic function $Z(\lambda/k)$ defined for $Im\lambda > 0$ as

$$Z(\lambda/k) = \pi^{-1/2} \int_{-\infty}^{\infty} \frac{e^{-x^2}\, dx}{x - \lambda/k} \tag{14}$$

and as its analytic continuation for $Im\lambda \leq 0$ as prescribed by the Landau contour . Evaluation of this function for $Im\lambda = 0$ ($\lambda = \lambda_r + i\lambda_i$; $\lambda_i = 0$) is obtained by using the Plemelj formula Eq. (9) and yields

$$Z(\lambda_r/k) = \pi^{-1/2}\ P\int_{-\infty}^{\infty} \frac{e^{-x^2}}{x-\lambda_r/k} + \pi^{1/2} i(\text{sgn}k) e^{-\lambda_r^2/k^2} . \tag{15}$$

Now observe that the integral in Eq. (5) may be written as

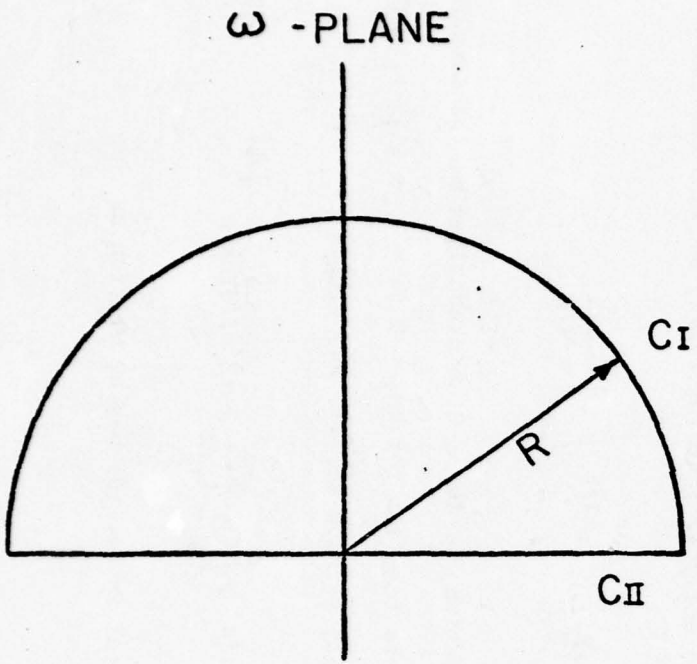

Fig. 2a Contour in the complex ω plane.

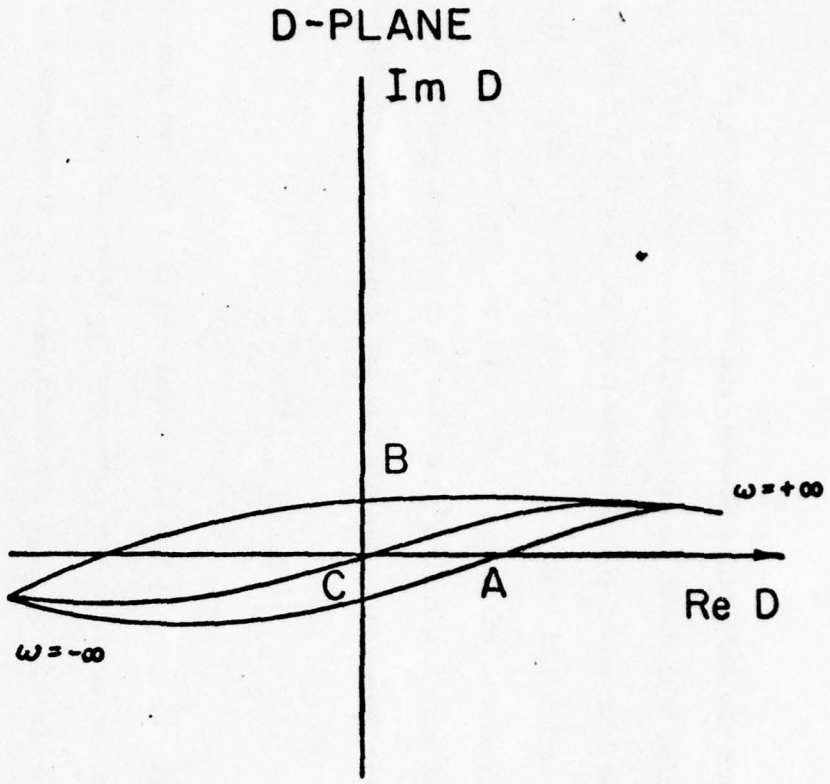

Fig. 2b Contour in the complex D plane.

$$\frac{1}{\sqrt{\pi}c_2}\int_{-\infty}^{\infty} du e^{-(u/c_2)^2}\ \frac{\Omega_{ci}-ku}{(\omega-kV_2+\Omega_{ci})} \;=\; 1+\left(\frac{\omega-kV_2}{kc_2}\right)Z\left(\frac{\omega-kV_2+\Omega_{ci}}{kc_2}\right)\ .$$

Now for $R \to \infty$, we note from properties of Z that

$$D(\omega) \sim \frac{\omega}{\Omega_{ci}} = \frac{R}{\Omega_{ci}} e^{i\theta}\ , \quad 0 \leqslant \theta \leqslant \pi\ ;$$

thus $[\text{Arg } D]C_I = \pi$. Therefore, in order that N be nonzero, we must require that

$$[\text{Arg } D]C_{II} = \pi(2n+1)\ ; \quad n = 0,1...$$

First we split D into its real and imaginary parts (for ω real):

$$\text{ReD} = (1-\eta)\frac{\Omega_{ci}}{\omega-kV_1+\Omega_{ci}} + \eta\left[1+\left(\frac{\omega-kV_2}{kc_2}\right)\text{ReZ}\left(\frac{\omega-kV_2+\Omega_{ci}}{kc_2}\right)\right] - 1 - \frac{k^2C_A^2}{\Omega_{ci}^2} + \frac{\omega}{\Omega_{ci}} \qquad (16)$$

$$\text{ImD} = \frac{\omega-kV_2}{kc_2}\,\text{ImZ}\left(\frac{\omega-kV_2+\Omega_{ci}}{kc_2}\right) \qquad (17)$$

We now note that for $\omega \to \pm\infty$ we have

$$\text{ReD} \sim \omega/\Omega_{ci} \to \pm\infty$$

and

$$\text{ImD} \sim \pi^{1/2}(\omega/|k|c_2)\ \exp(-\omega^2/k^2c_2^2) \to \pm\varepsilon$$

so that the point representing D in the complex D-plane traverses a curve from $-\infty - i\varepsilon \to +\infty + i\varepsilon$ as ω traverses C_{II}. From Eq. (17) we see that this point crosses the real D axis once only, at $\omega = kV_2$ so that three distinct curves in the D-plane may be traced as ω traverses C_{II}. These are shown in

Fig. 2b as A, B, and C and are keyed to the sign of ReD at the point for which ImD = 0. In summary, for $\omega = kV_2$ and ImD = 0,

$$\text{A} \quad \text{ReD} > 0 \Rightarrow [\text{Arg D}]C_{II} = \pi \Rightarrow N = 1 \text{ (Instability)},$$

$$\text{B} \quad \text{ReD} < 0 \Rightarrow [\text{Arg D}]C_{II} = -\pi \Rightarrow N = 0 \text{ (Stability)},$$

$$\text{C} \quad \text{ReD} = 0 \Rightarrow \text{(Marginal Stability)}.$$

Thus we see that the domain of instability will be determined by the condition that ReD ≥ 0 for $\omega = kV_2$, with the equality sign giving the stability-instability boundary in the U-k plane for an arbitrary beam strength η. Now substituting $\omega = kV_2$ into ReD gives the instability criterion

$$(1-\eta)\frac{k^2U^2/\Omega_{ci}^2}{1 - k|U|/\Omega_{ci}} - \frac{k^2C_A^2}{\Omega_{ci}^2} \geq 0 \tag{18}$$

where $|U| = -U$ for the negative drift case considered here. Two observations are immediately seen: (i) for $k|U| > \Omega_{ci}$ $(k > 0)$, there will be unconditional stability for all beam strengths, and (ii) for $\eta \to 1$, there can be no instability unless $U \to \infty$ and $k < 0$. Thus for a cold beam-hot plasma configuration, instability will only occur for modes propagating antiparallel to $\underset{\sim}{B}_o$ generated by a large relative streaming velocity. Observations (i) and (ii) thus imply that unstable whistlers may exist for finite U only if $|U| < \Omega_{ci}/k$ and $\eta < 1$. With these constraints on $|U|$ and η the relevant inequality for instability becomes

$$M_D \geq H(x,\eta) \tag{19}$$

where

$$H(x,\eta) = -\frac{x}{2(1-\eta)} + \left[\frac{1}{1-\eta} + \frac{x^2}{4(1-\eta)^2}\right]^{1/2}, \tag{20}$$

$$M_D = |U|/C_A , \quad x = kC_A/\Omega_{ci} .$$

A simple asymptotic analysis of Eq. (20) shows that

$$\lim_{\eta \to 1} H(x,\eta) = \begin{cases} 1/x & x > 0 \\ \infty & x < 0 \end{cases}$$

so that as η varies between 0 and 1 the curves of marginal stability, $M_D = H(x,\eta)$, fill the region between $M_D = H(x,0)$ and $M_D = 1/x$ $(x > 0)$. Thus for a given beam strength, the domain of M_D-x pairs for which instability may occur is given by the inequality

$$H(x,\eta_o) \lesssim M_D \lesssim 1/x .$$

and is represented graphically as the region between the curves $H(x,\eta_o)$ and $1/x$. Plots of $H(x,\eta)$, for various values of η, and $1/x$ are shown in Fig. 3. Note that for $\eta << 1$ the marginal stability curve is simply related to the negative branch of the whistler dispersion curve ν_{o-} by

$$M_D = -\frac{x}{2} + \left[1 + \frac{x^2}{4}\right]^{1/2} = -\frac{1}{x}\,\frac{\nu_{o-}}{\Omega_{ci}}$$

in agreement with the results of Sec. II.A. and Eq. (11).

III. APPLICATION TO PARALLEL SHOCK WAVE STRUCTURE

The analysis of the preceding section can now be applied to the structure of parallel shocks. We determine both the spectrum of unstable modes that may exist at various points in the interior of the shock as well as which of these modes are stationary in the rest frame of the shock leading edge. In this

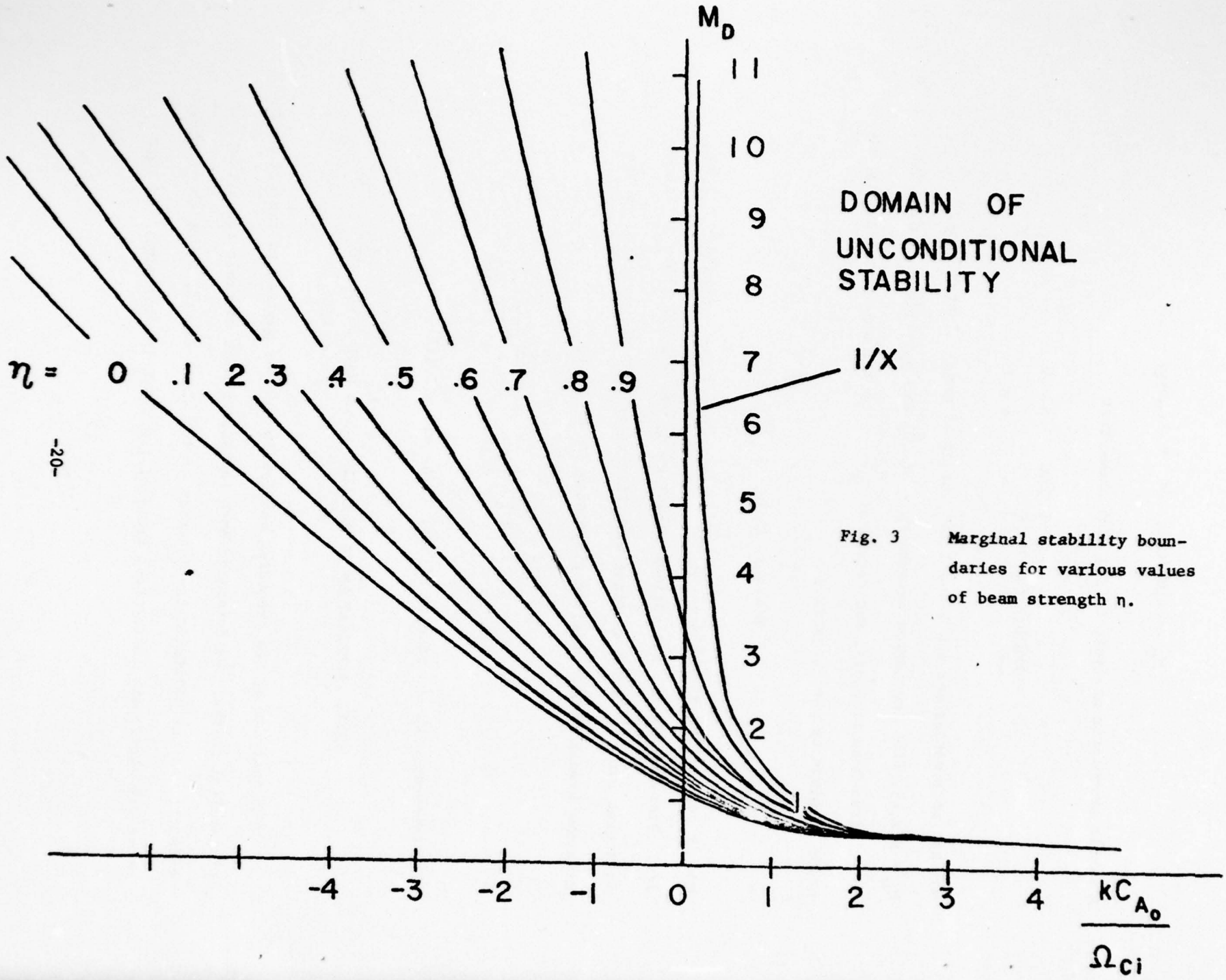

Fig. 3 Marginal stability boundaries for various values of beam strength η.

work the cold ion stream requirement of the previous theory[2] is partially relaxed by allowing the shocked, downstream ions to have a Maxwellian velocity distribution with temperature T_d and mass velocity $\underset{\sim}{V}_d$ dictated by the conservation relations applied across the shock wave. The unshocked, upstream ions are assumed to be very cold compared to the downstream ions and are moving with mass velocity $\underset{\sim}{V}_u$. The shock layer is now modelled as a superposition of these up- and downstream ion beams moving with relative velocity $\underset{\sim}{U} = \underset{\sim}{V}_d - \underset{\sim}{V}_u$ and with beam strength $\eta(z)$ dependent on position in the shock layer. Using the Mott-Smith assumption that the velocity distribution in the interior of a shock wave be a bimodal Maxwellian then leads to the ion distribution in the shock layer in the form

$$f_i(z,\underset{\sim}{v}) = n_u(z)\delta(\underset{\sim}{v}-\underset{\sim}{V}_u) + n_d(z)(\pi C_d^2)^{-3/2} \exp[-(\underset{\sim}{v}-\underset{\sim}{V}_d)^2/C_d^2]$$

where $C_d^2 = 2\kappa T_d/m_i$ (κ = Boltzmann's constant) and $n_{u,d}(z)$ represent the up- and downstream ion densities respectively at a point z in the shock layer. The warm background electrons move with mass velocity $\underset{\sim}{V}_e(z) = [1-\eta(z)]\underset{\sim}{V}_u + \eta(z)\underset{\sim}{V}_d$ where $\eta(z) = n_d(z)/[n_u(z) + n_d(z)]$ dictated by the requirements of local charge and current neutrality. For simplicity $n_u(z)$ is assumed to decrease linearly from its upstream value $n_{u\infty}$ at the shock leading edge to zero at the trailing edge whereas $n_d(z)$ is assumed to increase linearly from zero at the shock leading edge to its downstream value $n_{d\infty}$ at the trailing edge. A schematic of the density distribution is sketched in Fig. 4[2].

The valid dispersion relation is now obtained from Eq. (5) by Doppler shifting the frequency ω according to

$$\omega_s = \omega + \underset{\sim}{k}\cdot\underset{\sim}{V}_e \qquad (21a)$$

and by transforming all velocities from the electron- to shock-frame according

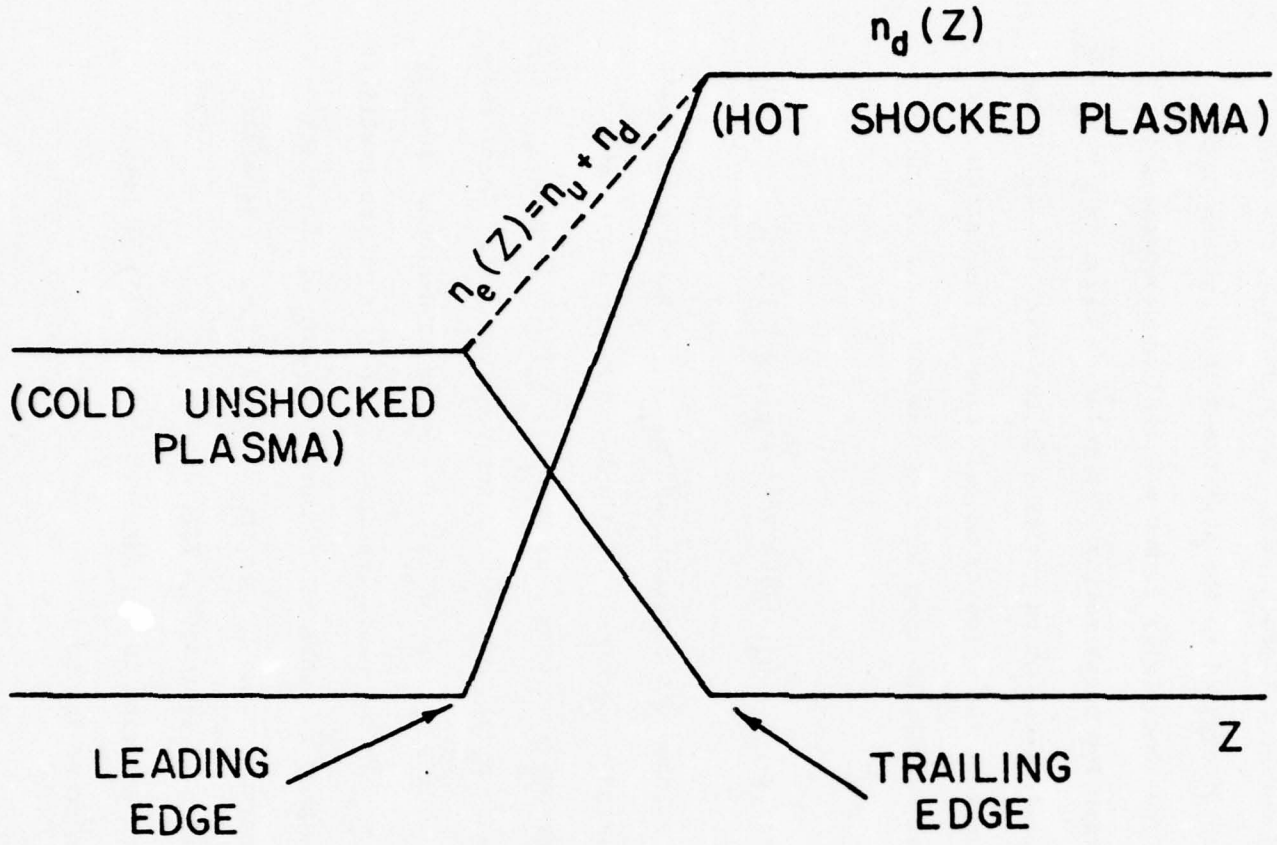

Fig. 4 Sketch of total ion density in the shock indicating upstream and downstream components as well as the assumed linear variation through the shock.

to

$$\underset{\sim}{V}_u = \underset{\sim}{V}_1 + \underset{\sim}{V}_e \tag{21b}$$

$$\underset{\sim}{V}_d = \underset{\sim}{V}_2 + \underset{\sim}{V}_e \tag{21c}$$

By substituting these into Eq. (5) we obtain

$$D(\omega_s,k) = [1-\eta(z)]\,\frac{\Omega_{ci}}{\omega_s - kV_u + \Omega_{ci}} + \eta(z)\left[1 + \left(\frac{\omega_s - kV_d}{kC_d}\right) Z\left(\frac{\omega_s - kV_d + \Omega_{ci}}{kC_d}\right)\right]$$

$$-1 - \frac{k^2 C_A^2(z)}{\Omega_{ci}^2} + \frac{\omega_s}{\Omega_{ci}} - \frac{kV_e(z)}{\Omega_{ci}} = 0 \tag{22}$$

The solution of Eq. (22), $\omega_s = \omega_s(k)$, will provide the spectrum of unstable growth modes for a particular shock position z and given shock strength, $V_u - V_d$. Only those growth modes which are stationary in the shock rest frame (i.e. have zero group velocity) are of interest, since only these modes have sufficient time to grow to large amplitude to scatter incoming ions. The analysis of growth and group velocity of these modes is again separated into two parts: (i) the shock leading edge ($\eta << 1$), and (ii) arbitrary points in the shock interior ($0 \leq \eta \leq 1$). In addition, the leading edge calculation has been extended to include the effects of finite temperature in the unshocked, upstream ions.

A. Leading Edge Analysis ($\eta(z) << 1$, Cold Upstream Plasma)

The leading edge analysis proceeds in the same way as the weak beam analysis of Sec. II. Setting $\omega_s = \nu_s + i\gamma_s$, $0 < \gamma_s << |\nu_s|$ and performing a perturbation expansion for both γ_s and η small leads to the solution

$$\nu_s(k;V_u) = kV_u + k^2C_{Ao}^2/2\Omega_{ci} - kC_{Ao}[1 + (kC_{Ao}/2\Omega_{ci})^2]^{1/2} , \qquad (23a)$$

$$\frac{\gamma(k;V_u)}{\Omega_{ci}} = \eta \frac{\sqrt{\pi}}{|k|C_d} \frac{(\nu-kV_u+\Omega_{ci})^2(kV_d-\nu)}{(\nu-kV_u)(\nu-kV_u+2\Omega_{ci})} \exp\left[-\frac{(\nu-kV_d+\Omega_{ci})^2}{k^2C_d^2}\right] \qquad (23b)$$

Strong interaction evidently corresponds to the intersection of the $\nu - kV_d + \Omega_{ci} = 0$ hot ion beam line with the cold whistler dispersion curve, Eq. (23a), in the third quadrant of the (ω_s,k)-plane. Here the resulting γ_{max} varies directly with the strength η of the hot beam. In the previous theory[2], where the shocked ions were modelled as a cold energetic beam, the corresponding weak ion beam-whistler interaction was found to be stronger, i.e. $\gamma_{max} \propto \sqrt{\eta}$. This is not surprising since, in the present theory, the whistler wave interacts strongly only with a small percentage of the hot beam ions, whereas in the previous theory, all of the particles in the mono-energetic ion beam participate in the interaction.

From Eq. (23b), we see that instability (i.e., $\gamma > 0$) is possible only if $kV_d - \nu(k;V_u) > 0$; this together with (22) gives $\gamma > 0$ for

$$\frac{V_u - V_d}{C_{Ao}} > \frac{|k|C_{Ao}}{2\Omega_{ci}} + \left[1 + \frac{k^2C_{Ao}^2}{4\Omega_{ci}^2}\right]^{1/2} . \qquad (24)$$

V_d, however, is connected to V_u through the gasdynamic Rankine-Hugoniot relation

$$\frac{V_d}{V_u} = \frac{M_A^2 + 3}{4M_A^2} , \quad (M_A = V_u/C_{Ao}, \quad C_p/C_v = 5/3) \qquad (25)$$

where, to avoid the possibility of "switch-on" type shocks[3], we have assumed $C_{Ao} = C_{su} = 5\kappa T_u/3m_i$. Equations (24) and (25) combine to give the leading edge

instability condition

$$M_A > \frac{2}{3}g + (1 + \frac{4}{9}g^2)^{1/2} , \tag{26}$$

$$g = -\frac{x}{2} + (1 + \frac{x^2}{4})^{1/2} , \quad x = \frac{kC_{Ao}}{\Omega_{ci}} , \quad C_{Ao} = C_A(0) .$$

Next from Eq. (23a) the zero group velocity condition is easily found to be

$$M_A = -x + (1 + \frac{x^2}{4})^{1/2} + \frac{x^2}{4}(1 + \frac{x^2}{4})^{-1/2} . \tag{27}$$

A sketch of the stability-instability boundary [Eq. (26)] and the locus of zero group velocity modes [Eq. (27)] is shown in Fig. 5 plotted in the $(M_A, |x|)$ plane. Evidently, for a given Mach number $M_A \gtrsim 2.77$, the shocked hot ion-cyclotron beam mode can drive unstable a particular whistler mode which, in the rest frame of the shock front, is stationary near the leading edge. This whistler can therefore grow to large amplitude there and ultimately couple the upstream and downstream plasma flows. Thus the turbulent whistler mode structure for intermediate strength shocks ($M_A \gtrsim 5.5$) suggested by the previous cold beam[2] theory is suggested as well for weak shocks ($2.77 \lesssim M_A \lesssim 5.5$) by the present hot beam theory.

B. Effects of Finite Upstream Temperature on the Structure of the Shock Leading Edge

These leading edge conclusions are modified somewhat by including in the analysis the effects of finite upstream temperatures. The valid dispersion relation in this case contains two singular integrals of the form found in Eq. (22). To obtain some indication of temperature effects in the unshocked

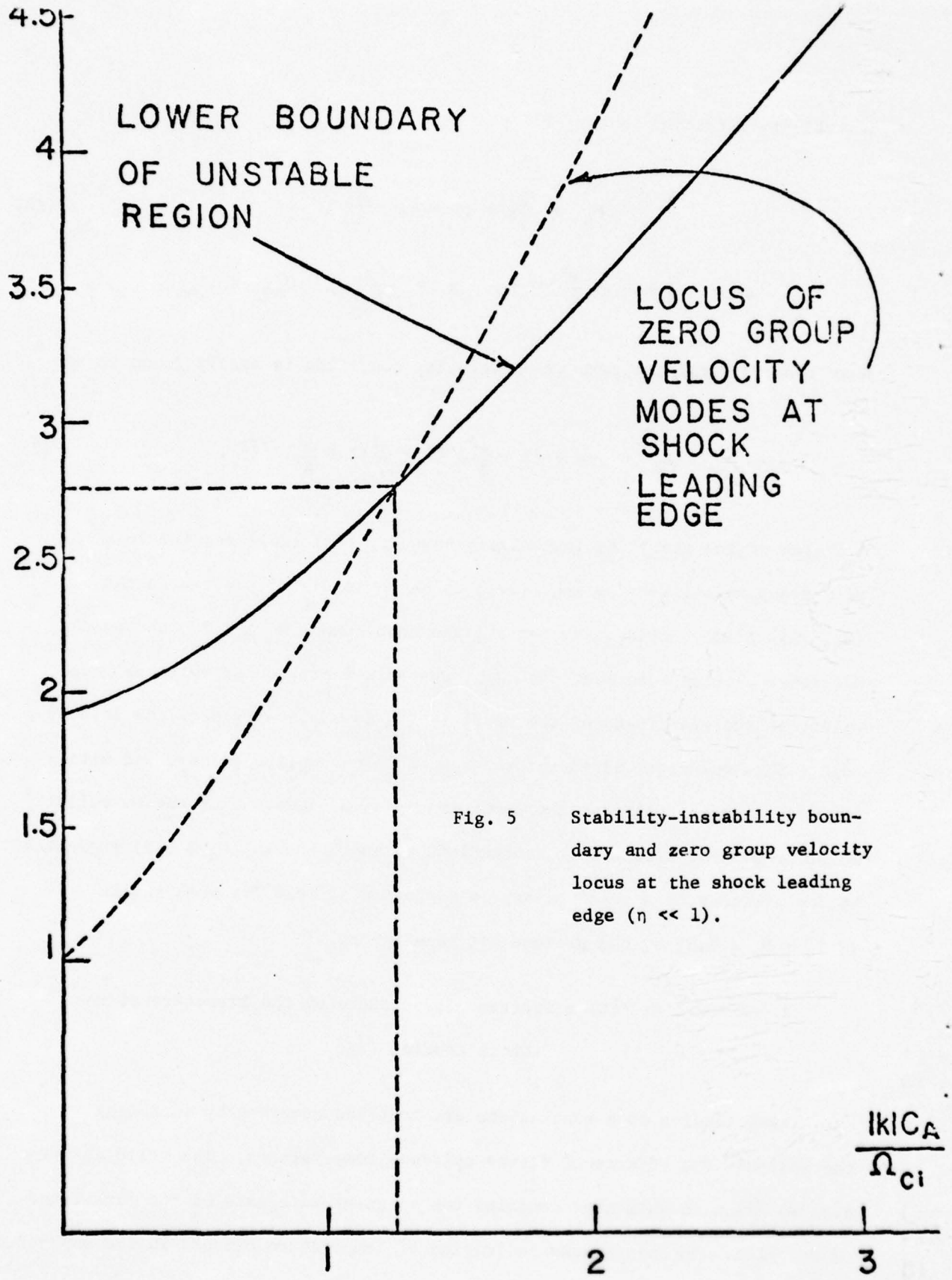

Fig. 5 Stability-instability boundary and zero group velocity locus at the shock leading edge ($\eta \ll 1$).

plasma an approximate analysis has been performed in which the upstream plasma thermal speed, C_u, is finite but sufficiently small so that

$$k^2C_u^2 \ll 2(\nu_s - kV_u + \Omega_{ci})^2 . \tag{28}$$

This approximation results in limiting lowest order upstream thermal effects to the imaginary part of $D(\omega_s, k)$ only. Thus the zeroth order approximation to ν_s is again given by the whistler dispersion formula, Eq. (23a). In addition, it is assumed that in the imaginary part of $D(\omega_s, k)$, both damping and growth effects occur to the same order, leading to a growth rate γ of the form

$$\frac{\gamma}{\Omega_{ci}} = (\eta-\eta_c) \frac{\sqrt{\pi}}{|k|C_d} \left|\nu_s+|k|V_d\right| \exp\left[\frac{(\nu_s+|k|V_d+\Omega_{ci})^2}{k^2C_d^2}\right] \tag{29}$$

and with the instability criterion ($k < 0$)

$$\nu_s < -|k|V_d. \tag{30}$$

which is identical to that given by Eq. (24). Consequently, the stability-instability boundary is again given by Eq. (26) is shown in Fig. 5. Furthermore, in Eq. (29), η_c represents a critical penetration distance into the shock before which ($\eta < \eta_c$) the effects of damping dominate growth but beyond which instability again occurs. Some simple calculations indicate that for $M_A \geq 3$, Eq. (28) is well satisfied and $\eta_c < .05$, so that the approximate calculation is consistent with the leading edge small perturbation theory. Consequently, the effects of finite upstream heating (sufficient e.g. to prevent the occurrence of switch-on shocks, but small enough so that Eq. (28)

is sa ed) is to cause a small portion of the shock interior to be stable to the two stream disturbance. The conditions for the instability to occur are then both Eq. (30) and $\eta > \eta_c$. For the range of shock parameters of interest, however, $\eta_c < .05$ so that the principle results of this section are unaffected.

C. Shock Layer Analysis ($0 < \eta < 1$, Cold Upstream Plasma)

The previous analysis of the shock leading edge has demonstrated that relatively weak shocks ($M_A \geq 2.77$) can be structured by this Whistler mode instability since for all shock Mach numbers larger than 2.77, there can exist unstable whistlers that are stationary (have zero group velocity) in the shock rest frame. The results of Sec. II indicate that for all beam strengths unstable whistlers can be generated by sufficiently large relative beam drift. Consequently, it can be inferred that at all points of the shock interior, unstable whistler modes may exist. Since the instability criterion as given in Eq. (18) is invariant with respect to the transformation of Eqs. (21), the criterion for the shock interior may be written as

$$[1 - \eta(z)] \frac{k^2U^2/\Omega_{ci}^2}{1 - k|U|/\Omega_{ci}} - \frac{k^2C_A^2(z)}{\Omega_{ci}^2} \geq 0 \qquad (31)$$

where $|U| = V_u - V_d$ and the variation of η and C_A with position in the shock layer is explicitly noted. Furthermore, applying Eqs. (21) to the Nyquist criterion $\omega = kV$ leads to

$$\omega_s = kV_d. \qquad (32)$$

Therefore for points on the boundary of instability (equality in Eq. (31)), ω_s is real and is given by Eq. (32) for all positions in the shock layer. Again it may be observed for Eq. (31) that instabilities may exist for finite drift only if $k|U| < \Omega_{ci}$ $(k > 0)$ and $\eta < 1$. Thus trailing edge instabilities may exist only for infinitely strong shocks. With these restrictions on $|U|$ and η, the relevant condition can be recast as

$$|U| > -\left[\frac{1}{1-\eta(z)}\right]\frac{kC_A^2(z)}{2\Omega_{ci}} + \left[\frac{C_A^2(z)}{1-\eta(z)} + \frac{k^2C_A^4(z)}{4[1-\eta(z)]^2\Omega_{ci}^2}\right]^{1/2} \tag{33}$$

with the equality defining the surface of marginally stable modes.

Now within the framework of the Mott-Smith Formalism, the shock is considered to be a superposition of upstream and downstream plasmas with beam densities $n_u(z)$ and $n_d(z)$ at any point in the shock with relative drift velocity $|U| = V_u - V_d > 0$. For simplicity the density in the shock is assumed to be linear in z so that $n_e(z)$ may serve to define the fraction of penetration into the shock, ζ, as

$$\zeta = \frac{n_e(z) - n_{u\infty}}{n_{d\infty} - n_{u\infty}}$$

where $n_{u\infty}$ and $n_{d\infty}$ are the plasma densities in the uniform regions before and after the shock and $n_e(z)$ the total plasma density at the point z in the shock. Thus $\zeta = 0, 1$ refer to leading and trailing edge conditions respectively. Using the definition of $n(z) = n_d(z)/n_e(z)$ then leads to

$$\zeta = \frac{\eta}{\eta + \tau(1 - \eta)} \tag{34}$$

where $\tau = n_d/n_u = V_u/V_d$ is the shock compression ratio expressed in terms of

M_A by Eq. (25). Therefore,

$$1 - \eta(z) = (1 - \zeta)\left[1 + 3\zeta\,\frac{M_A^2 - 1}{M_A^2 + 3}\right]^{-1} \tag{35}$$

Furthermore, the variation of Alfvén speed through the shock can be expressed in terms of leading edge conditions by the relation

$$\frac{C_A^2(z)}{C_{Ao}^2} = \frac{n_{u\infty}}{n_e(z)} = \left[1 + 3\zeta\,\frac{M_A^2 - 1}{M_A^2 + 3}\right]^{-1} = \frac{1 - \eta(z)}{1 - \zeta} \; . \tag{36}$$

Since the relative velocity $|U| = V_u - V_d$ may be referred to the upstream Alfvén Mach number M_A through the Rankine Hugoniot conditions for a parallel shock wave as

$$\frac{V_u - V_d}{C_{Ao}} = \frac{3(M_A^2 - 1)}{4M_A} \tag{37}$$

Eq. (33) can be written solely in terms of M_A, k, and ζ as follows:

$$M_A > \frac{2}{3}g + \left[1 + \frac{4}{9}g^2\right]^{1/2} \equiv F(k, \zeta) \tag{38a}$$

where

$$g = -\frac{kC_{Ao}}{2(1 - \zeta)\Omega_{ci}} + \left[\frac{1}{1 - \zeta} + \frac{1}{4}\,\frac{k^2 C_{Ao}^2}{(1 - \zeta)^2 \Omega_{ci}^2}\right]^{1/2} \; . \tag{38b}$$

In addition, the region of unconditional stability ($k|U| < \Omega_{ci}$ for $k > 0$) can be rewritten as

$$M_A < \frac{2}{3}\frac{\Omega_{ci}}{kC_{Ao}} + \left[1 + \frac{4}{9}\frac{\Omega_{ci}^2}{k^2 C_{Ao}^2}\right]^{1/2} \equiv G(k) . \qquad (39)$$

Plots of $F(k, \zeta)$ and $G(k)$ are given in Fig. 6. A simple asymptotic analysis of Eqs. (38) shows that for $\zeta \to 1$ we have the two results

$$\lim_{\zeta \to 1} F(k, \zeta) = G(k); \quad k > 0$$

$$\lim_{\zeta \to 1} F(k, \zeta) = \infty; \quad k < 0 ,$$

so that the family of curves given by $F(k, \zeta)$ fills the region between $\zeta = 0$ and the boundary of unconditional stability given by $G(k)$.

The result is that in the M_A-k space of Fig. 6 at a particular shock position ζ, the domain of unstable modes must lie between the corresponding ζ curve and the curve of unconditional stability. Furthermore, as $\zeta \to 1$, this domain vanishes rapidly. Our principle result, however, is that although unstable whistlers may exist at all points of the shock layer, very high M_A are required for such instabilities near the shock trailing edge. Although some of these modes will be stationary (have vanishing group velocity in the shock rest frame), it seems certain that the weakest shocks will have unstable whistlers with zero group velocity only near the leading edge.

This latter conclusion can be strengthened by considering the group velocity of unstable modes at each shock position as a function of shock Mach number M_A. In particular on the marginal stability surface (MSS), for which

$$M_A = F(k, \zeta) \qquad (40)$$

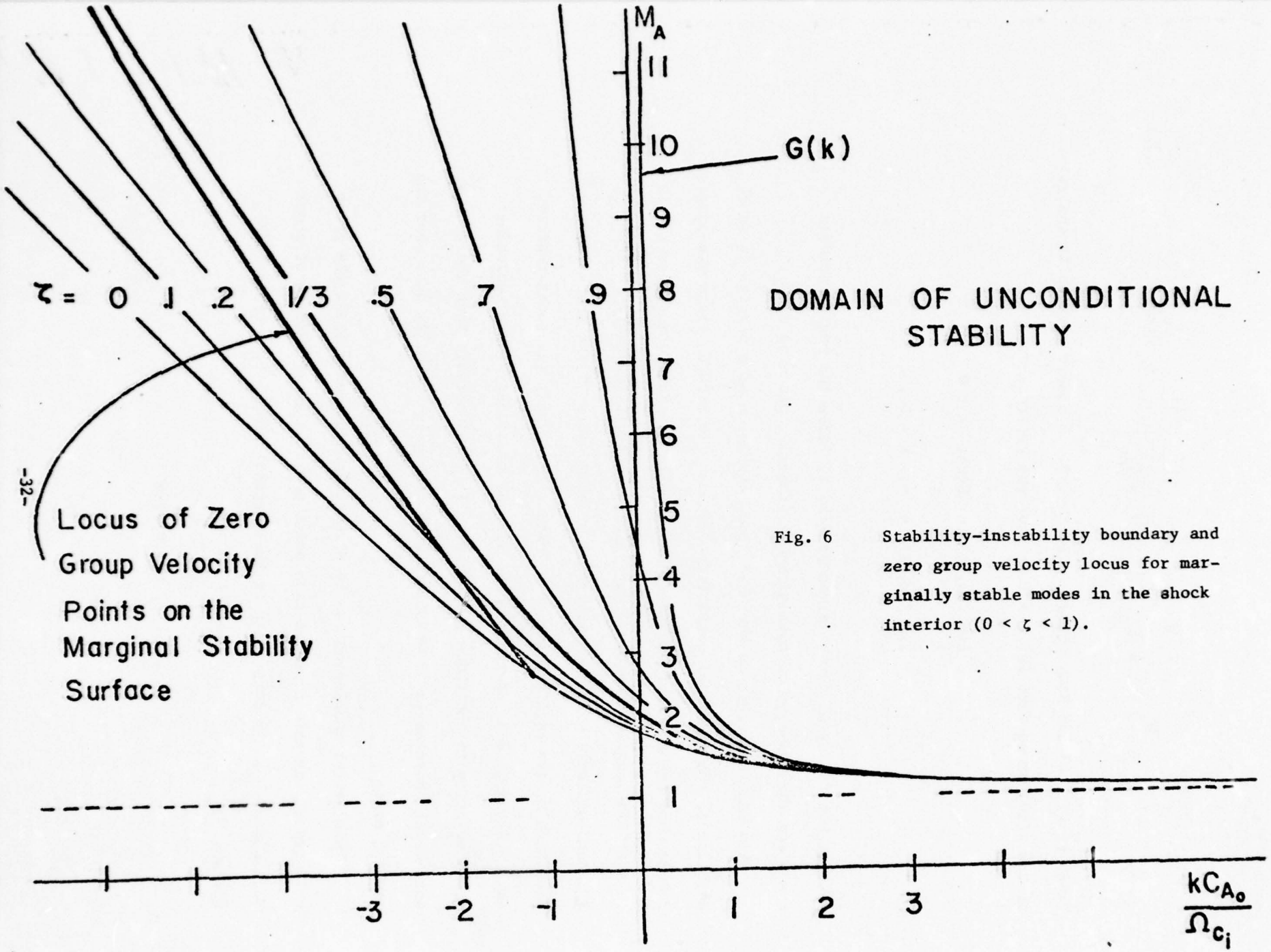

Fig. 6 Stability-instability boundary and zero group velocity locus for marginally stable modes in the shock interior ($0 < \zeta < 1$).

with $F(k, \zeta)$ given by Eqs. (38), the locus of points for which the group velocity vanishes can be found from the linear dispersion relation as given by Eq. (22). The first step in the analysis is to set $\omega_s = \nu_s + i\gamma_s$ and to perform a Taylor series expansion of ν_s and γ_s about points on the MSS. Therefore we have

$$\nu_s = \nu_s^* + \left(\frac{\partial \nu_s}{\partial k}\right)^* (k - k^*) = k^* V_d + k^* V_g^* \delta \tag{41}$$

$$\gamma_s = \gamma_s^* + \left(\frac{\partial \gamma_s}{\partial k}\right)^* (k - k^*) = \Gamma^* \delta \tag{42}$$

where

$$\begin{aligned} k &= k^*(1 + \delta) \quad ; \quad \delta << 1 \\ \nu_s^* &= k^* V_d \quad ; \quad V_g^* = \left(\frac{\partial \nu_s}{\partial k}\right)^* \\ \gamma_s^* &= 0 \quad ; \quad \Gamma^* = k^* \left(\frac{\partial \gamma_s}{\partial k}\right)^* \end{aligned} \tag{43}$$

and (*) denotes quantities evaluated on the MSS. After substituting Eqs. (41) and (42) into the real and imaginary parts of Eq. (22), we find (i) that the zeroth order terms in the δ ordering vanish identically after using Eq. (40), and (ii) to within $O(\delta)$ we have

$$(1-\eta) \frac{k^*(V_u - V_g^*)\Omega_{ci}}{(k^*U - \Omega_{ci})^2} - \eta \frac{k^*(V_d - V_g^*)}{\Omega_{ci}} R_1 - \eta \frac{\Gamma^*}{\Omega_{ci}} I_1 - 2 \frac{k^{*2} C_A^2(z)}{\Omega_{ci}^2}$$

$$- \frac{k^*(V_u - V_g^*)}{\Omega_{ci}} + \eta \frac{k^* U}{\Omega_{ci}} = 0 \tag{44}$$

$$\frac{\Gamma^*}{\Omega_{ci}} = \frac{k^*(V_d - V_g^*) I_1}{\left\{1 - (1-\eta)(1 - \frac{k^*U}{\Omega_{ci}})^{-2} + \eta R_1\right\}} \tag{45}$$

In these expressions R_1 and I_1 are related to the real and imaginary parts of Z for real argument by the equations

$$R_1 = \frac{\Omega_{ci}}{|k^*C_d|} Z_r\left(\frac{\Omega_{ci}}{|k^*C_d|}\right) ; \quad I_1 = \frac{\Omega_{ci}}{|k^*C_d|} Z_i\left(\frac{\Omega_{ci}}{|k^*C_d|}\right)$$

where $Z = Z_r + iZ_i$. In principle, Eqs. (44) and (45) can be solved to give the group velocity of any marginally stable mode, $V_g^* = V_g^*(k^*, \zeta)$. In particular the locus of stationary, marginally stable modes is determined by setting $V_g^* = 0$ in Eqs. (44) and (45) and solving for the resulting $k^* - \zeta$ pairs. Equations (25) and (35-40) can be used to express $n(z)$, V_u, and V_d in terms of k^* and ζ. Furthermore, the arguments of R_1 and I_1 can be written as

$$\frac{\Omega_{ci}}{|k^*C_d|} = \frac{\Omega_{ci}}{|k^*|C_{Ao}} \frac{C_{Ao}}{C_d} = \frac{\Omega_{ci}}{|k^*|C_{Ao}} \sqrt{\frac{5}{6}\frac{T_u}{T_d}}$$

where we have used $C_{Ao}^2 = 5\kappa T_u/3m_i$ to avoid switch-on shocks. The ratio T_u/T_d can be obtained via momentum and energy conservation across the shock as

$$\frac{T_u}{T_d} = \frac{48M_A^2}{15M_A^4 + 42M_A^2 - 9} .$$

Using these relations in Eqs. (44) and (45) leads ultimately to an equation of the form

$$x^* = C(x^*, \zeta) , \quad x^* \equiv -\frac{k^*C_{Ao}}{\Omega_{ci}} \tag{46}$$

where

$$C(x^*, \zeta) = [C_1(x^*, \zeta) - 1]/M_D$$

$$C_1(x^*, \zeta) = \left[\frac{3}{8}(1 - \zeta)(M_A^2 - 1)(2 + x^*M_D) + C_2(x^*, \zeta)\right]^{1/2}$$

$$C_2(x^*, \zeta) = \frac{1}{2}\frac{\zeta M_A}{x^*}(1 + x^*M_D)^2 C_3(x^*, \zeta) \qquad (47)$$

$$C_3(x^*, \zeta) = 1 + R_1 + I_1^2/C_4(x^*, \zeta)$$

$$C_4(x^*, \zeta) = 1 + \left[4\frac{M_A^2\zeta R_1}{M_A + 3} - \frac{(1 - \zeta)}{(1 + x^*M_D)^2}\right] C_5(x^*, \zeta)$$

$$C_5(x^*, \zeta) = \left[1 + 3\zeta\frac{M_A^2 - 1}{M_A^2 + 3}\right]^{-1}$$

Equation (46) has been solved numerically for $x^*(\zeta)$ by a convergent iterative procedure. The results are shown as a locus of points on Fig. 6. Furthermore, Fig. 7 shows a plot of M_A vs. ζ for which marginally stable modes are stationary in the rest frame of the shock. Figures 6 and 7 demonstrate that M_A and k^* both become unbounded as $\zeta \to 1/3$. An asymptotic expansion of Eqs. (47) for $M_A >> 1$, $x^* >> 1$ leads to the expression

$$C(x^*, \zeta) \sim A(\zeta)x^* + B(\zeta)/x^*$$

where

$$A = (2/3)^{1/2}(1 - \zeta)^{-1/2}$$

and

$$B = (1 - \zeta)\left\{\frac{5}{\sqrt{6}}(1 - \zeta)^{3/2} + (\frac{3}{8})^{3/2}(1 - \zeta)^{5/2} - 1\right\} .$$

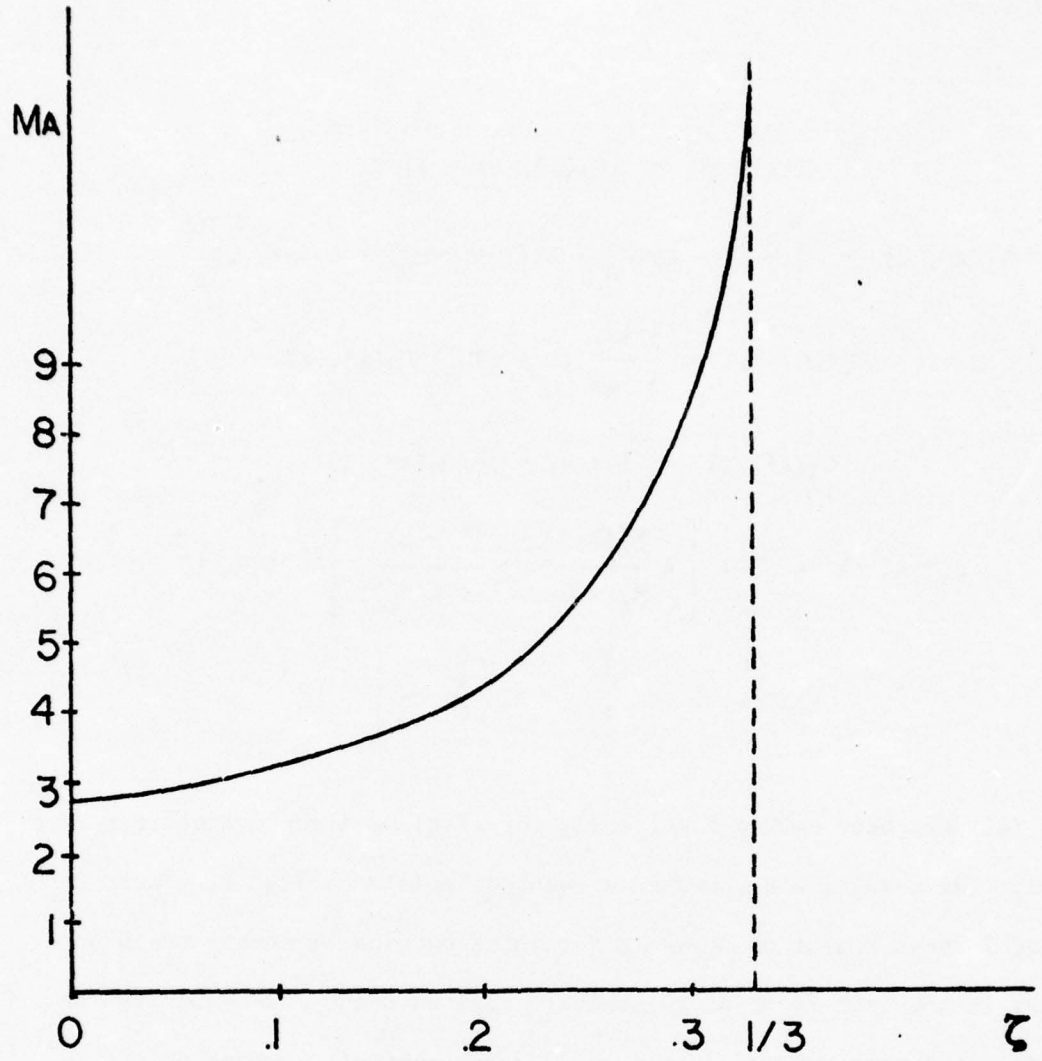

Fig. 7 Range of Alfvén Mach numbers for which unstable whistlers are stationary in the shock frame vs. shock position ζ.

The solution of Eq. (46) then becomes

$$k^* = -\frac{\Omega_{ci}}{C_{Ao}}\left(\frac{B}{1-A}\right)^{1/2}$$

where the unphysical positive solution has been discarded. Note that Eq. (48) becomes unbounded as $\zeta \to 1/3$ from below and that no real solution for k^* exists for $\zeta \geq 1/3$. This is consistent with our numerical solution of Eq. (46) as shown in Figs. 6 and 7. The existence of these stationary unstable whistler modes for $0 \leq \zeta < 1/3$ significantly extends the previous cold theory[2], for which unstable whistlers were stationary only for $0 \leq \zeta < .1$. This result strengthens the previous conclusion of Golden et. al.[2] that this two stream instability is an important source of turbulent dissipation required to structure a collisionless parallel shock wave.

IV. DISCUSSION AND CONCLUSIONS

The instability generated by two ion beams counterstreaming with relative velocity U and beam strength η parallel to an external magnetic field $\underset{\sim}{B}_o$ and in the presence of a charge and current neutralizing electron background has been analyzed using linear dispersion theory. The previous cold beam theory of Golden et. al.[2] has been extended by allowing one of the ion beams to have a finite temperature in order to model a collisionless shock wave more realistically. By using the Nyquist method[5], a family of curves in the normalized U vs. k space has been obtained, which represents the locus of marginally stable whistlers parametrized by the beam strength η ($0 \leq \eta < 1$). The instability for $\eta << 1$ may be interpreted as a hot ion

cyclotron beam mode driving unstable a cold plasma whistler mode. The detailed analysis for $\eta << 1$ results in a growth rate $\gamma \propto \eta$ in contrast to the previous cold beam-cold plasma theory in which a typical hydrodynamic result, $\gamma \propto \eta^{1/2}$, was obtained.

A collisionless shock wave has also been modelled by using a Mott-Smith bimodal Maxwellian assumption for the ion velocity distribution in the shock rest frame with constant up- and downstream temperatures throughout the shock wave but with linearly varying densities. Each point, ζ, in the shock then serves as an appropriate environment for the two stream instability under consideration, where here the beam strength $\eta(\zeta)$ is a measure of position in the shock. We have obtained the family of curves of marginal stability parametrized by shock position ζ in the M_A vs. k space. Superimposed on these curves in the locus of marginally stable modes which are stationary in the shock rest frame. It has been found that for a given M_A, stationary unstable whistlers may exist at all points in the shock from the leading edge, $\zeta = 0$, to the interior point, $\zeta = \zeta_M < 1/3$ as given by Fig. 7. These modes have time to grow to large amplitude and will determine the turbulent spectrum for a given shock strength (M_A). From Figs. 5 and 6 we can determine for a given M_A the wave numbers of the leading edge and ζ_M modes. We have found that for all $M_A \geq 2.77$, these two wave numbers differ by approximately 2%. This suggests that for a given shock strength, the turbulent spectrum has a very narrow band width and is located near the wave number of the unstable, stationary leading edge mode.

The principle differences between the previous cold theory[2] and the present work are:

(i) weaker leading edge growth rate characteristic of Vlasov plasmas,

(ii) existence of unstable stationary whistlers for weaker shocks ($2.77 \leqslant M_A$) than in the previous theory ($5.5 \leqslant M_A$),

(iii) the region of instability extends to arbitrarily large shock strengths but was bounded above in the previous theory, and

(iv) unstable and stationary modes may exist for a larger range of shock positions ($0 \leqslant \zeta < 1/3$) than previously ($0 \leqslant \zeta < .1$).

The effects of finite upstream temperature, T_u, have been considered in a simple way since to avoid switch-on shocks[3] it has been assumed that $5\kappa T_u/m_i = C_{Ao}^2$. We have found that for the range of shock Mach numbers under consideration the results of our cold upstream theory remain essentially valid even for a finite but small T_u (Sec. III.B.). The effects of obliquely propagating modes ($\underset{\sim}{k} \not\parallel \underset{\sim}{B}_o$) and nonlinear saturation on parallel shock structures are currently under consideration and will be reported in a later paper.

V. ACKNOWLEDGMENTS

It is a pleasure to acknowledge helpful discussions with G. Kalman and the assistance of D. Chiaverini and A. Voyatzakis.

REFERENCES

1. M.S. Kovner, Zh. Eksp. Teor. Fiz. 40, 527 (1961).

2. K.I. Golden, L.M. Linson, and S.A. Mani, Phys. Fluids 16, 2319 (1973).

3. A.R. Kantrowitz and H.E. Petschek, in Plasma Physics in Theory and Application, edited by W.B. Kunkel (McGraw-Hill, New York, 1966) p. 148.

4. R.L. Briggs, Electron Stream Interactions in Plasmas (M.I.T. Press, Cambridge, Massachusetts, 1964) p. 83.

5. N.A. Krall and A.W. Trivelpiece, Principles of Plasma Physics (McGraw-Hill Inc., New York, 1973).

C. CALCULATION OF ENERGETIC PARTICLE FLUXES

I. *INTRODUCTION*

A principal objective of this research is to investigate the effects of high altitude nuclear bursts on energetic charged particle injection into the earth's magnetosphere. The work reported in Sec. B has identified a particular two stream instability that can serve as the necessary dissipative mechanism to structure a collisionless shock wave. This instability occurs in the loss cone exits of an existing nuclear debris bubble as the expanding debris from a second detonation passes over the ionized ambient air plasma. The importance of this result is that since any finite amplitude wave passing over a stationary plasma has a tendency to put the originally stationary plasma into motion, the passage of a debris structured collisionless shock wave through the ionized ambient air in the loss cone corridor will serve to accelerate these ions along the distended geomagnetic lines and thus generate particle fluxes into the magnetosphere.

In order to apply the results of our theory to the calculation of these fluxes, we consider the environment generated by two high altitude Starfish-like nuclear bursts (Fig. 1). We show first that for these parameters unstable whistlers traveling with the shock exist and have sufficient time to grow to large amplitude while passing over roughly 60% of the loss cone corridor. Therefore, this emphasizes the relevance of the theory presented in Sec. B. to the deposition of energetic particles into the magnetosphere.

Explicit calculations of the number of such particles are performed using three different approaches. It will be seen that all three approaches yield the same order of magnitude although based on different physical assumptions about the shock dynamics after shock formation.

II. GROWTH RATES FOR STARFISH PARAMETERS

Consider the multiple burst environment as shown in Fig. 1. If a second Starfish-like nuclear burst occurs inside of an already existing nuclear debris bubble (of extent $\sim$ 1000 km), a fraction of the second bomb's debris will be injected directly into the loss cone exits of the parent bubble.

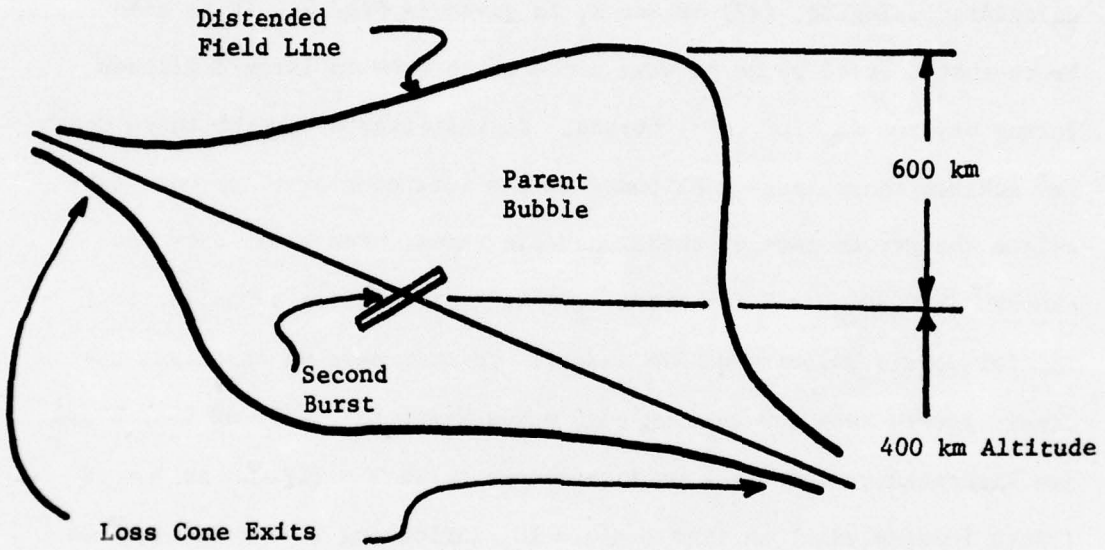

Figure 1

The number of such debris particles which enter a loss cone exit depends critically on the mass and orientation of the second bomb casing just prior to the burst. In the loss cone corridor, the debris plasma drives a shock wave. This shock is structured by unstable whistler waves which stand at its leading edge. To verify that these whistler modes can grow to sufficiently large amplitude to scatter incoming air ions (as viewed in the reference frame of the shock front), we require that the non-dimensional parameter $\gamma\, \ell/u > 1$, where $\ell \sim 500$ km is a characteristic length of

travel of the debris particles in the loss cone corridor. During daylight burst conditions the density of oxygen ions is $n_{O^+} \sim 10^5$-10^6, the larger value reflecting maximum sunspot activity. For an ambient field strength $B \sim 0.3$ gauss, this corresponds to an Alfven speed $C_A \sim 163$ - 516 km/sec in the ambient air plasma.

For typical initial casing velocities of from 500 km/sec to 2000 km/sec the initial Alfvén Mach numbers are from 1.96 to 12.22. A summary of the spectrum of stationary unstable leading edge whistlers, calculated using Eq. (27) of Sec B. is given in Fig. 2. It is seen there that a broad range of wave numbers can grow to large amplitude during daytime ($n \sim 10^6$ cm^{-3}) bursts. To investigate whether these modes can achieve these large amplitudes in the loss cone exit, we must calculate the growth rate of these unstable waves. For simplicity we choose $|k|C_A/\Omega_{ci} = 2$ for which $M_A = 4.12$, indicating a realistic initial debris velocity of 674 km/sec. In this case we calculate the linear growth rate for leading edge modes using Eqs. (23) of Sec. B and the Rankine-Hugoniot shock wave relations to be $\gamma = 167\ \eta$. At $\eta = .2$ (shock leading edge) we find $\gamma\ \ell/u = 10$, indicating 10 e-folding times pass as the shock traverses 500 km of the loss cone corridor. Thus the $|k| = 2\ \Omega_{ci}/C_A$ unstable whistler modes can grow to sufficiently large amplitude after traveling 500 km along the loss cone corridor to pick up background air plasma. The air electrons are rapidly accelerated by ensuing ion-electron electrostatic instabilities. Since the calculation is based on the lower bound of M_A, it is clear that 10 e-folding times in 500 km is a conservative estimate since stronger shocks will have larger growth rates.

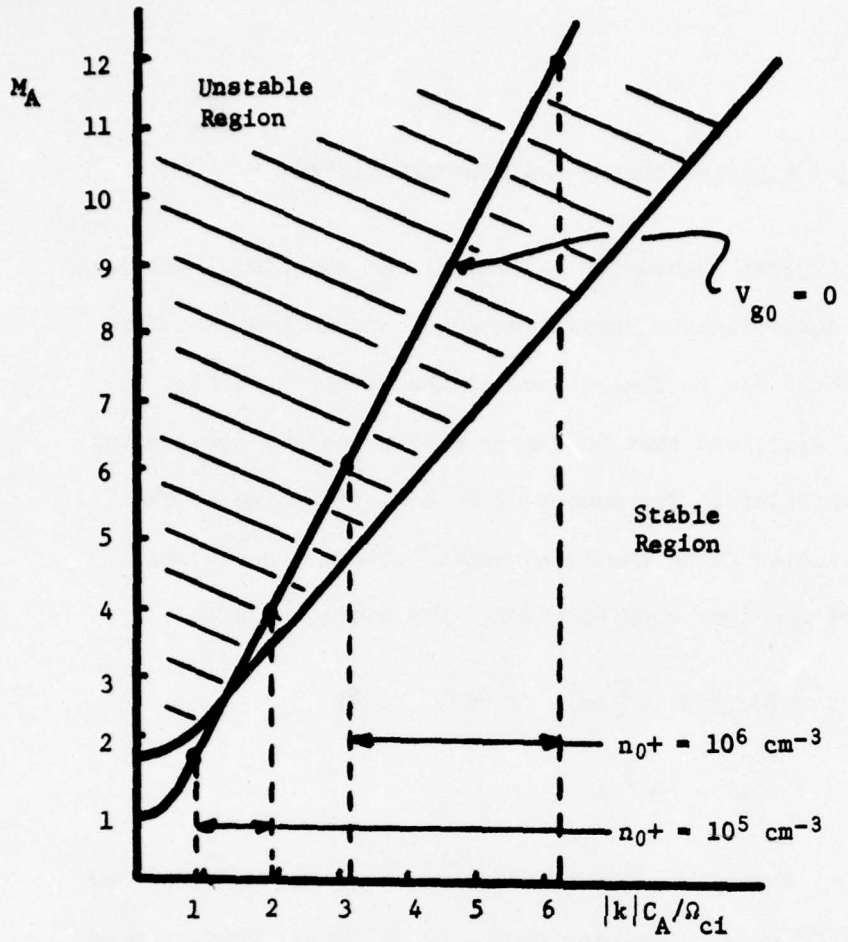

B_o = .3 gauss at 400 km altitude

Ω_{ci} = 180S^{-1} for 0^+ ions

	1,000 km/sec	2,000 km/sec
$n_o + = 10^6$ cm^{-3} C_A = 164 km/sec	$M_A = 6.1$ $\frac{k C_A}{\Omega_{ci}} = 3.05$	$M_A = 12.2$ $\frac{k C_A}{\Omega_{ci}} = 6.1$
$n_o+ = 10^5$ cm^{-3} C_A = 516 km/sec	$M_A = 1.94$ $\frac{k C_A}{\Omega_{ci}} = .9$	$M_A = 3.88$ $\frac{k C_A}{\Omega_{ci}} = 1.94$

Figure 2

III. CALCULATIONS OF PARTICLE DEPOSITION

Perhaps the simplest method for estimating the additional particle deposition due to collisionless mechanisms is to assume that the loss cone corridor is about 850 km long (based on the geometry of Fig. 1. See also Zinn, et. al.), and that 500 km is needed for the development of the turbulent whistlers. The number of 0^+ ions picked up by the debris ions is estimated to be the total number of air ions in the remaining 350 km of the loss cone corridor. Therefore, we have:

$$N_f \text{ (loss cone)} \begin{cases} = (0.35 \times 10^8 \text{ cm}) \quad (\text{A cm}^2) \quad (10^5) \\ = 0.35 \times 10^{13} \text{ A} \end{cases}$$

where A is the cross sectional area of the loss cone exit and where we have taken $n_{o^+} \sim 10^5$ cm^{-3}. Assuming that A is 1% of the surface area of the parent debris bubble, i.e. $A \sim .01\ (4\pi R^2) \sim 1.13 \times 10^{14}$ cm^2 (for $R \sim 300$ km), we have that N_f (loss cone) $\sim 0.4 \times 10^{27}$ 0^+ ions. For an iron bomb weighing 10^6 gm, $N_{Fe} \sim 10^{28}$, only a fraction of these particles would be blown into the loss cone exit. It is, therefore, likely that air ions comprise certainly no less than 10% of the plasma deposited into the Van Allen belts by direct injection of nuclear debris from a second burst into the loss cone exit of a parent debris bubble. It is possible, however, that this figure could be much larger, perhaps 100% depending on the fraction of the second bomb debris being directly injected into the loss cone exit, the length of the loss cone corridor, and the actual initial debris velocity.

The length of the loss cone corridor in which shock-produced acceleration of ambient ions occurs is determined ultimately by the distance the shock travels before attenuating to a low strength. We now modify our previous estimate by including this attenuation. In this calculation we assume the debris to expand outward from the second burst into the existing loss cone corridors of the parent bubble. We know that the debris-ambient ion interaction provides an environment for a two stream instability that can be stationary in the leading edge of a propagating shock wave. Consequently, we assume the result of this debris motion is to form a shock in the loss cone corridor. The conservation equations for this collisionless shock are unaffected by the magnetic field ($\perp$ to shock plane). So as an estimate of the shock dynamics we can consider only a gas dynamic shock (if we neglect switch-on type shocks). Thus we assume that a piston of mass/unit area m with a velocity V_o moves into stationary gas at conditions p_o, ρ_o, $u_o = 0$, $C_o = C_A$ (C_o = sonic velocity). At $t = 0$, the piston first impacts the ambient gas (Fig. 3).

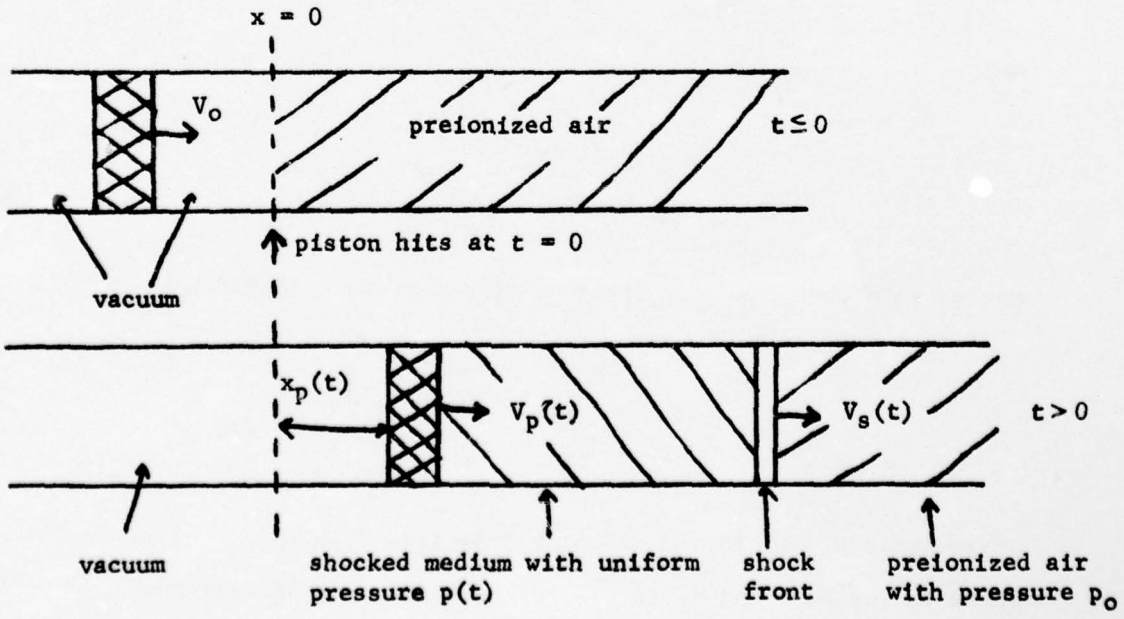

Figure 3

The result of this impact is to drive a shock wave into the ambient gas that moves with speed $V_s(t)$. This has the effect of decelerating the piston by means of the pressure p(t) exerted on the piston faces. So

$$m\ddot{x}_p(t) = -p(t) \tag{1}$$

Now we assume that this pressure can be given by

$$\frac{p(t)}{P_o} = \frac{2\gamma M_s^2}{\gamma+1} - \frac{\gamma-1}{\gamma+1} \tag{2}$$

(pressure ratio across a normal shock)

If this approximation is to hold, i.e. that p(t) on the piston face is the same as p behind the advancing shock, it is necessary to assume that the sound speed behind the shock is large, i.e. the shock is very strong. Therefore

$$M_s >> 1 \tag{3}$$

and

$$\frac{p(t)}{Po} \cong \frac{2\gamma M_s^2}{\gamma+1} \tag{4}$$

Now we know that the velocity jump across a shock is given by

$$-\frac{[w]}{c_1} = \frac{2}{\gamma+1}\left(M_1 - \frac{1}{M_1}\right) \approx \frac{2}{\gamma+1} M_1 \tag{5}$$

where $[w] = w_2 - w_1$ is the velocity jump (see figure 4), c_1 is the sound speed in region 1 and M_1 is the upstream (i.e. unshocked) Mach number in the shock front rest frame.

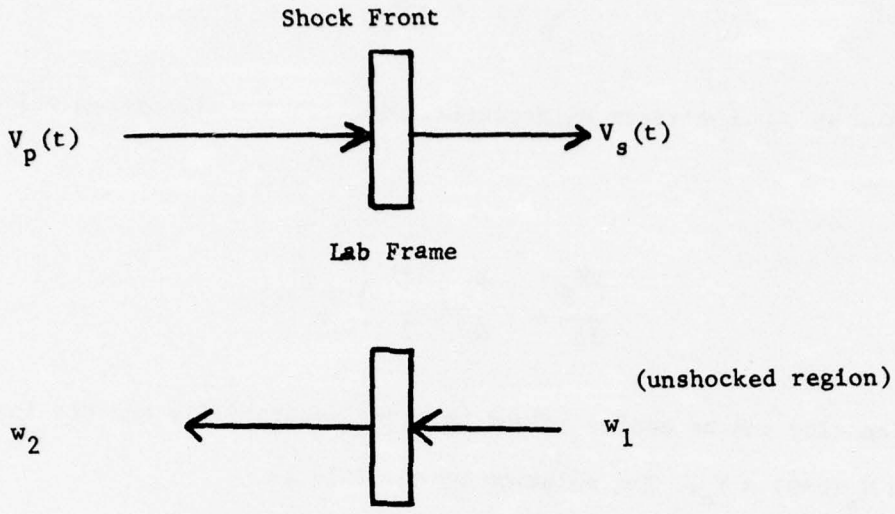

Figure 4

For our case it is seen that

$$c_1 = c \ , \ w_1 = V_s \ , \ w_2 = V_s - V_p, \ M_1 = M_s(t) \text{ and } [w] = V_p(t) \tag{6}$$

and so from (5) we find

$$\frac{V_p(t)}{c_o} = \frac{2}{\gamma+1} M_s(t) \tag{7}$$

Using eq. (7) in eq. (2) we obtain

$$p(t) = \rho_o \left(\frac{\gamma+1}{2} \right) V_p^{\,2}(t) \tag{8}$$

where we used

$$c_o^{\,2} = \gamma \, P_o/\rho_o \tag{9}$$

From eqs. (1), (8), and the fact that

$$\ddot{x}_p(t) = \frac{dV_p(t)}{dt} \tag{10}$$

we arrive at a nonlinear differential equation for the piston velocity $V_p(t)$

$$\frac{dV_p}{dt} = -\frac{\rho_o}{m}\left(\frac{\gamma+1}{2}\right) V_p^{\,2}(t) \tag{11}$$

Equation (10) can be easily solved by using separability and the initial condition $V_p(t=0) = V_o$. The solution of eq. (11) is

$$V_p(t) = \frac{V_o}{1 + \frac{\rho_o V_o}{m}\left(\frac{\gamma+1}{2}\right) t} \tag{12}$$

Now we assume that the shock will stop picking up particles when the shock mach number $M_s(t)$ reaches a mach number $M_f \sim 2.76$. This will occur at a time t_f. From eqs. (7) and (12) we find that

$$t_f = \frac{m}{\rho_o c_o M_f} - \frac{m}{\rho_o v_o}\frac{2}{(\gamma+1)} \sim \frac{m}{\rho_o c_o M_f} \tag{13}$$

where eq. (3) was used.

From this attenuation time t_f one can obtain the effective loss-cone corridor length ℓ_f over which pickup occurs. This is given by

$$\ell_f = \int_o^{t_f} V_s(t)dt \tag{14}$$

From eqs. (7) and (12) we obtain

$$f = \frac{m}{\rho} \ell n \left[1 + \frac{V_o}{C_A} \frac{1}{M_f} \frac{\gamma + 1}{2} \right] \quad . \tag{15}$$

Noting that $\ell f \rho_o$ is the mass pickup per unit area m_f and that $\ell_n \left[1 + \frac{V_o}{C_A} \frac{1}{M_f} \frac{\gamma + 1}{2} \right]$ is of order unity, we find

$$m_f \equiv \ell \rho_o \sim m = \text{mass per unit area of the piston} \tag{16}$$

Thus the debris piston is predicted to pick up its mass in air ions.

Before examining some typical numbers, we note that this model describes an attenuation mechanism which is quite different from a momentum conservation or "snowplow" type model. For purposes of comparison we shall present the snowplow idea and then calculate some relevant quantities using both models.

For a momentum conserving system of piston plus picked-up air, we can write

$$V_p(t) = \frac{mv_o}{m+m_a(t)}$$

where $m_a(t)$ is the mass of air pickup per unit area at time t. If we use a strong shock approximation, i.e. eq. (7), we obtain

$$M_s(t) = \frac{\gamma + 1}{2} \frac{m}{m + m_a(t)} \frac{V_o}{C_A} \quad . \tag{18}$$

When pickup ceases $M_s(t) = M_f$, $m_a(t) = m_f$ and we find

$$m_f = m \left[\frac{\gamma + 1}{2} \frac{V_o}{M_f C_o} - 1 \right] \sim \frac{\gamma + 1}{2} \frac{V_o}{M_f C_A} m \quad . \tag{19}$$

If we now compare the two models we find

$$\frac{m_f \text{ (Gas Dynamic Slowdown)}}{m_f \text{ (Snowplow)}} = \frac{2}{(\gamma+1)} \frac{M_f}{M_{Ao}} \tag{20}$$

with

$$M_{Ao} = \frac{V_o}{C_A} \tag{21}$$

From (20) it is clear that m_f (Snowplow) gives the higher pickup (we shall see it is typically four times larger for a starfish-like environment).

Typical Numerical Results

We make the assumption that the loss cone exit comprises 1% of the parent bubble area A_b ($\sim 1.13 \times 10^6$ km^2) and so <u>total</u> debris piston mass M_p is

$$M_p = (.01)M_b = (.01)(10^3 \text{ kg}) = 10 \text{ kg} \tag{22}$$

Assuming

$$V_o = 1000 \text{ km/sec} \tag{23a}$$

$$C_{Ao} = 160 \text{ km/sec} \tag{23b}$$

$$\gamma = 5/3 \tag{23c}$$

we find that the total number N of <u>oxygen ions</u>, 0^+, picked up will be

$$N_f \text{ (Gas Dynamic Slowdown)} \equiv .01A_b \frac{m_f}{M_{0^+}} = .4 \times 10^{27} \text{ particles} \tag{24}$$

$$N_f \text{ (Snowplow)} = .6 \times 10^{27} \text{ particles} \tag{25}$$

If V_o were 2000 km/sec, estimate (24) would not change significantly due to the 0(1) property of the ℓn function (see eq. (15))while

$$N_f \text{ (Snowplow)} = 1.65 \times 10^{27} \text{ particles} \tag{26}$$

IV. COMPARISON OF BURST FLUXES WITH MAGNETOSPHERIC SUBSTORM FLUXES

In the past few years there has been considerable concern over the phenomena of synchronous orbit satellites charging to high potentials as a result of magnetospheric substorms (Rosen, 1975). These substorms consist of the injection of high energy plasma, with characteristics as shown in Figure 5, from the earth's magnetotail into the region of synchronous orbit. This injection process is shown in Figure 6. Those portions of a satellite subject to the high energy plasma will charge to a potential several times the electron energy while other portions of the satellite will remain at ground potential. Potentials near ground are maintained by photoelectron emission from illuminated surfaces on the spacecraft or by contact with the ambient low energy plasma.

During eclipse photoelectron emission disappears and during a substorm the ambient low energy plasma flux is strongly dominated by the injected high energy plasma. The most damaging discharges as a result of spacecraft charging probably occur between shadowed spacecraft components influenced by substorm plasma and illuminated components at ground potential. When the discharge passes through electrical circuitry between the components, damage can result. Electromagnetic interference can also result from surface discharges and considerable surface deterioration can be caused by arcing.

The following discussion will be an assessment of the possible spacecraft charging effects which can result from the large scale transport of ionospheric plasma to synchronous orbit by nuclear bursts. The plasma instability explored in the previous sections of this report demonstrates

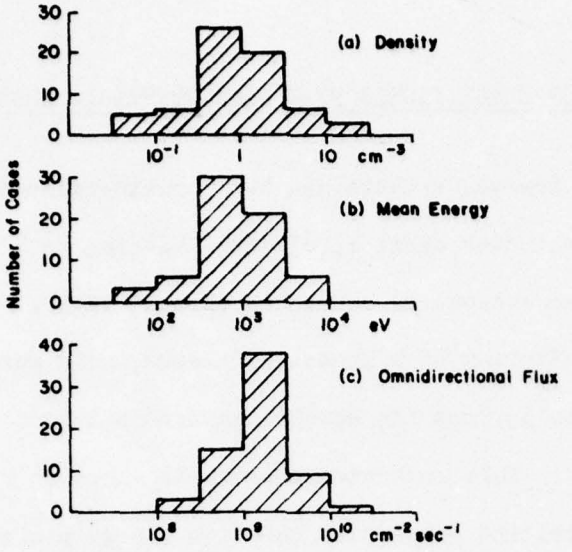

Figure 5 Typical Plasma Electron Characteristics as Measured in the Plasma Sheet. These are the electron properties attributed to the midnight to dawn portion of synchronous orbit during a substorm [After Vasyliunas (1968)]

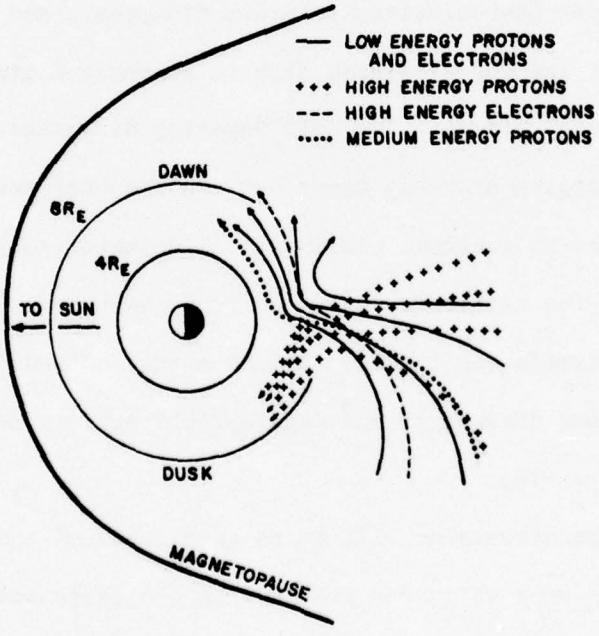

Figure 6 Average Particle Motions for Various Energies and Particle Types during a Substorm Plasma Injection from the Magnetotail [After DeForest and McIlwain (1971)]

a mechanism for structuring a collisionless shock wave. This mechanism will operate during a high altitude nuclear burst as the expanding nuclear debris passes over the stationary ionospheric plasma. Through the interaction of large amplitude whistler mode waves, plasma will be picked up by the collisionless shock and accelerated into the magnetosphere.

As the large mass of debris and plasma propagates along the earth's magnetic field lines, the plasma mass will tend to expand as the field lines expand at high altitudes. This is illustrated in Figure 7.

Using nuclear burst parameters for a Starfish-like (nominally 1.5 megaton) burst (Zinn, 1966) the previous calculations have conservatively estimated that near 1×10^{27} O^+ ions would be carried by the shock when 1% of the total debris exits the loss cone. Depending on orientation, mass, and shape of the bomb casing, this number could be considerably higher.

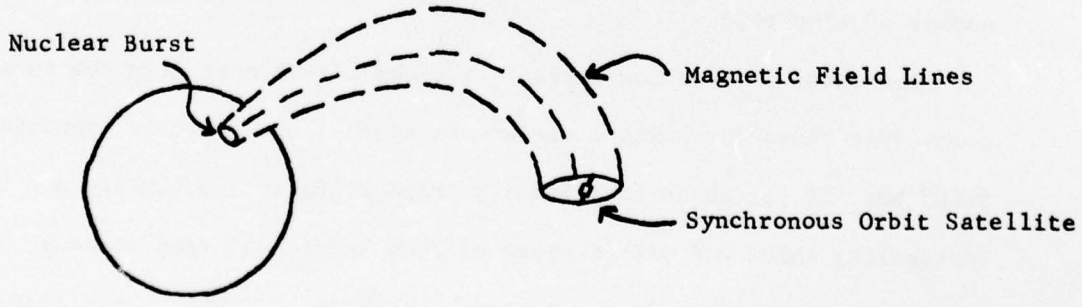

Figure 7. Nuclear Debris forms collisionless shock which transports Ionospheric Plasma to higher altitudes.

Conservative Worst Case Flux Estimates

The original objective of this research was to study the injection of plasma into the magnetosphere from multiple nuclear bursts and their interaction. The greatest yield of field aligned debris fluxes will probably come from the detonation of a nuclear burst inside the already formed debris bubble from a previous burst. If the bomb casing is cylindrical and with its axis oriented along the magnetic field lines, near 50% of the debris could exit the loss cone. At higher altitudes and at night, there would be a great proportion of the ionospheric plasma in the form of H^+ with a mass of one-sixteenth that of O^+. The debris shock would be able to accumulate significantly more of this plasma prior to turnoff of the instability. A conservative worst case estimate of the total ion pickup might be $1x10^{29}$ ions, with more than an order of magnitude contributed by the proper multi-burst scenario and less than an order of magnitude contributed by H^+ pickup. Plasma neutrality and electron mobility will quickly insure that the plasma contains an equal number of electrons.

The total propagation distance for the plasma mass from the burst point just above the earth's surface to synchronous orbit is approximately $5x10^4$ km. If the shock is initially propagating at 2000 km/sec and the instability shuts off with a speed of 1000 km/sec and free streams, it will take greater than 50 sec to reach synchronous orbit. This time is many ion cyclotron periods at all altitudes and sufficient to have thermalization of the complete plasma mass at near the ion temperature as the mass slows and diffuses (Biskamp, 1973).

The final shock velocity after instability cutoff and free streaming (an estimated 500 km/sec for higher altitudes) corresponds to an O^+ energy of approximately 20 keV. Little of this energy would be lost in thermalizing the mobile electrons to an equivalent energy.

The shock structure most likely forms with a spatial extent as found by (Zinn, 1966) and as mentioned previously of 500 km along the field lines and of 30 km radius perpendicular to the field lines for the loss cone. Over North America the field lines for synchronous orbit intersect the earth near a magnetic latitude of 67°N and the loss cone spreads over one degree of latitude.

One degree of latitude at 67°N will span an L shell difference of .5 (L = 6.3 to L = 6.8). At synchronous orbit this difference corresponds to a circular area of expansion for the loss cone of $A_f = 8 \times 10^6$ km^2. While the light masses of the electrons will allow rapid thermalization, the heavy masses of oxygen and particular the iron debris, will constrain their initial motion closely to the field lines and slow crossline diffusion. The outward diffusion of plasma caused by plasma pressure and the diverging field lines will increase the radial scale perpendicular to the field line by a factor of about 30, and diffusion along the field lines should be of an equivalent degree.

This evaluation of the spacecraft charging environment from multiple nuclear bursts is therefore estimated to be a total of 10^{29} electrons of 20 keV energy. These electrons would be spread over an area of $A_f = 8 \times 10^6$ km^2 at synchronous orbit. They would be in a shock piston of length $L = 30 \times 500$ km $= 1.5 \times 10^4$ km that would have a duration at a synchronous satellite of $t = 1.5 \times 10^4$ km/500 km/sec = 30 sec.

Based on the previous assumptions as to the nature of plasma deposition by multiple nuclear bursts it is possible to compare these fluxes with observed magnetospheric substorm electron fluxes. A total of 10^{29} electrons spread through a volume of $V = A_{\zeta} \times L = 1.2 \times 10^{11}\ km^3$ gives a density of approximately 8×10^2 electrons/cm^3. This density at an energy of 20 keV translates to an omnidirectional flux of 6.7×10^{12} electrons/cm^2-sec. These fluxes are significantly greater than those encountered during a magnetospheric substorm, as shown in Figure 8. While the duration of the nuclear injection is much shorter than a typical substorm, studies (Rothwell, et al, 1976) indicate the charging process takes only fractions of a second.

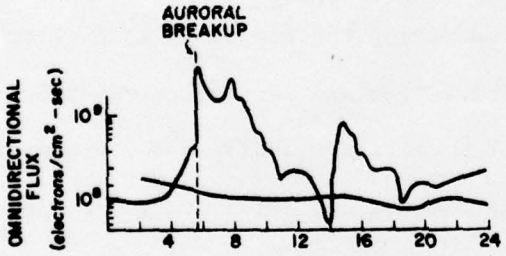

Figure 8 The Omnidirectional Flux of Electrons with Energies (650 eV < E < 53 keV) during a Substorm, with a Standard Reference Day for Comparison. [After Sharp and Johnson (1972)]

In both the single and multiple nuclear burst environments there appears to exist the potential for spacecraft charging effects at synchronous orbits. The calculated fluxes, densities, and energies of the injected electrons are all greater than those encountered during substorms and which have been observed to cause spacecraft charging.

These calculations contain many approximations, but until further research can refine the results it may be expected that synchronous

orbit satellites under certain nuclear burst conditions will find themselves subject to a short, but intense, period of spacecraft charging. Potentials in the tens of kilovolts for periods of tens of seconds are suggested. The resulting transient charging and arc discharging should surely be a part of the design criteria of any spacecraft expected to survive a situation where high altitude nuclear bursts are involved.

REFERENCES

1. Biskamp, D. (1973) "Collisionless Shock Waves in Plasmas", Nuclear Fusion, 13, 719.
2. DeForest, S. F., and C. E. McIlwain (1971) "Plasma Clouds in the Magnetosphere", J. Geophys. Res., 76 (No. 16), 3587.
3. Rosen, A. (1975) "Spacecraft Charging: Environment Induce Anomalies", AIAA Paper 75-91.
4. Rothwell, P. L., A. G. Rubin, A. L. Pavel and L. Katz (1976) "Simulation of the Plasma Sheath Surrounding a Charged Spacecraft", Proc. of Conference on Spacecraft Charging by Magnetospheric Plasmas, AIAA, (in press).
5. Sharp, R. D. and R. G. Johnson (1972) "The Behavior of Low-Energy Particles During Substorms", Plant. and Space Sci. 20 (No. 9), 1433.
6. Vasyliunas, V. T. (1968) "A Survey of Low-Energy Electrons in the Evening Sector of the Magnetosphere with OGO 1 and OGO 3, J. Geophys. Res., 73 (No. 9), 2839.
7. Zinn, T, H. Hoerlin, and A.Petachek (1966), "Motion of Bomb Debris Following the Starfish Test", Radiation Trapped in the Earth's Magnetic Field, edited by Billy McCormac (Gordon and Breach, New York).

D. DISCUSSION AND RECOMMENDATIONS

The results of this research have shown that a multiple nuclear burst can provide the necessary environment to excite an ion cyclotron beam mode-whistler mode two stream instability that is stationary in the rest frame of weak parallel shock waves. The expansion of debris from such bursts can therefore produce a collisionless shock wave in the loss cone corridors of an existing nuclear debris bubble. Estimates of the resulting electron fluxes along the distended geomagnetic field lines into the magnetosphere indicate that this mechanism could produce 20 kev omnidirectional electron fluxes of approximately 6.7×10^{12} cm^{-2} s^{-1} for durations as high as 30 s. These fluxes are two orders of magnitude larger than those due to magnetospheric substorms and occur for times one order of magnitude longer than that required for charging of synchronous orbit spacecraft. It would thus appear that multiple nuclear bursts could be a significant source of energetic particle fluxes into the magnetosphere and the cause of consequent charging of synchronous orbit spacecraft.

Since these conclusions are based on a linear dispersion theory of the relevant two stream instability and relatively simple calculations of particle fluxes caused by the passage of the resulting collisionless shock wave, two lines of further study are suggested:

(i) Continue the study of the hot ion cyclotron beam-whistler into the quasi-linear stage of its development with a calculation of the saturation level of the turbulence.

(ii) Improve calculations of particle fluxes by incorporating the results of the nonlinear study and by modelling the particle pick-up mechanism more realistically.

APPENDIX A

The attached Canadian Journal of Physics reprint summarizes our research on the magnetosonic two stream instability and its role in perpendicular shock wave structures.

NOTES

Crossfield Magnetosonic Two Stream Instability[1]

J. W. CIPOLLA, JR.[2] AND K. I. GOLDEN[3]

Northeastern University, Boston, Massachusetts 02115

Received January 14, 1975

In this article, a detailed analysis was made on the plasma magnetosonic instabilities whose propagation is perpendicular to the magnetic field and whose two streams cross the magnetic field during the time of development of the instability.

We have also studied the role of the magnetosonic instabilities in the structure of perpendicular shock waves. Since these instabilities are not stationary in the shock interior, one can ultimately deduce that they do not play a principal role in the structure.

Dans cet article, une analyse détaillée a été faite sur les instabilités magnétosonores de plasma dont la propagation est perpendiculaire au champs magnétique et dont les deux écoulements traversent le champs magnétique pendant le temps de developpement de l'instabilité.

Nous avons aussi étudié la rôle des instabilités magnétosonores dans la structure des ondes de choc perpendiculaires. Comme ces instabilités ne sont pas stationnaires à l'intérieur du choc, on peut en déduire finalment qu'elles ne jouent pas une rôle principale dans la structure.

Can. J. Phys., 53, 1022 (1975)

I. Introduction

The counterstreaming of two ion beams across a perpendicular magnetic field in the presence of a stationary electron background gives rise to a spectrum of unstable growth modes that were thought to provide the necessary turbulent dissipation to structure weak collisionless shock waves (Papadopoulos *et al.* 1971). In this note a complete study of this magnetosonic instability is presented, differing from the linear analysis of Papadopoulos *et al.* (1971) in that (*i*) the complete magnetosonic dispersion curve is used (resulting in a wider range of relevant drift Mach numbers), (*ii*) the weak beam – magnetosonic mode interaction is considered as well as the equidense beam theory, and (*iii*) pertinent calculations have been performed for the *e* folding growth lengths of unstable modes both at the leading edge and density midpoint of weak collisionless shock waves.

II. Linear Analysis

In this analysis, the two ion beams, with densities n_s and velocities V_s ($s = 1, 2$), are assumed to be unaffected by the magnetic field during the full development of the instability while the electrons are strongly bound to the field lines, so that the unperturbed system consists of two uniform beams with constant drift. The wave number and complex oscillation frequency therefore must satisfy

$$[1] \qquad k^2 a_e^2/\Omega_{ce}^2 \ll 1 \ll k^2 V_s^2/\Omega_{cs}^2; \quad \Omega_{cs}^2 \ll |\omega|^2 \ll \Omega_{ce}^2$$

where $\Omega_{cs(e)}$ is the ion (electron) cyclotron frequency. Furthermore, the parameter ordering is

$$[2] \qquad \Omega_{cs} \ll \omega \ll k a_e \ll \Omega_{ce} \ll \omega_{pe}; \quad \omega \ll kc; \quad \Omega_{cs} \ll |\omega - k V_s| \quad (s = 1, 2)$$

where $\omega_{ps(e)}$ is the ion (electron) plasma frequency and a_e is the electron thermal velocity. The

[1]Supported by the Air Force Cambridge Research Laboratories, Bedford, Massachusetts 01730, under contract number F19628-75-C-0012.

[2]Department of Mechanical Engineering, Northeastern University.

[3]Department of Electrical Engineering, Northeastern University.

perturbed plasma conductivity $\tilde{\sigma}$ is found from the linearized, Fourier transformed fluid equations for ions and electrons in conjunction with Faraday's law. Used in the dispersion relation,

$$\varepsilon_{xx} = \varepsilon_{xy}^2\omega^2/k^2c^2 \quad (\tilde{\varepsilon} = 1 + 4\pi i\tilde{\sigma}/\omega)$$

where x and y directions are taken along $V_s \| k$ and B_0 respectively, this in turn leads to the dispersion relation

$$[3] \qquad \frac{\omega_{p1}^2}{(\omega - kV_1)^2} + \frac{\omega_{p2}^2}{(\omega - kV_2)^2} = \frac{\omega_{pe}^2}{\Omega_{ce}^2}\left(1 + \frac{\omega_{pe}^2}{k^2c^2}\right)$$

In the electron rest frame, the charge and current neutrality condition of the unperturbed system can be incorporated into the single equation, $(1 - \eta)V_1 + \eta V_2 = 0$ where $\eta = n_2/n_1$ is the beam concentration. Then upon introducing into [3] the relative drift velocity $U = V_2 - V_1$ and the effective 'plasma frequency',

$$\omega_0(k) = [\Omega_{ce}\Omega_{ci}/(1 + \omega_{pe}^2/k^2c^2)]^{1/2}$$

one obtains,

$$[4] \qquad (1 - \eta)\omega_0^2(k)(\omega + \eta kU)^{-2} + \eta\omega_0^2(k)[\omega - (1 - \eta)kU]^{-2} = 1$$

In this convenient form both the weak ($\eta \ll 1$) and equidense ($\eta = 1/2$) beam theories may be analyzed.

Consider first $\eta \ll 1$. Setting $\eta = 0$ in [4] leads to the usual magnetosonic dispersion relation,

$$\omega = \omega_c(k) = kC_A(1 + k^2c^2/\omega_{pe}^2)^{-1/2}$$

where C_A is the local Alfvén speed. Possible strong interactions may be expected in the vicinity of the intersection of $\omega_0(k)$ with the beam dispersion curve $\omega_b = kU = kV_2$. Since the slope of $\omega(k)$ satisfies the inequality $\omega'(k) \leqslant \omega'(0) = C_A$, it is clear that such interactions can occur only if $M_d = U/C_A \leqslant 1$. A perturbation analysis of the full dispersion relation for $\eta \ll 1$ in the vicinity of the intersection shows that the spectrum of unstable modes is given by

$$0 \leqslant k^2 \leqslant (M_d^{-2} - 1)\omega_{pe}^2/c^2 \equiv k_c^2 \quad (M_d^2 \leqslant 1)$$

with maximum growth rate occurring at $k = k_c$ and given by

$$[5] \qquad \gamma = \mathrm{Im}\,(\omega) = \eta^{1/3}3^{1/2}2^{-4/3}[(1 - M_d^2)\Omega_{ci}\Omega_{ce}]^{1/2}$$

The equidense beam case can be analyzed by setting $\eta = 1/2$ and solving the resulting quartic equation for $\omega^2(k)$. It is found that for the k spectrum given by

$$0 \leqslant k^2 \leqslant (4M_d^{-2} - 1)\omega_{pe}^2/c^2 \quad (M_d = U/c_A)$$

ω is pure imaginary with growth rate

$$[6] \qquad \gamma(k) = \frac{\omega_0(k)}{2^{1/2}}\{[1 + 2M_d^2(1 + k^2c^2/\omega_{pe}^2)]^{1/2} - 1 - (1/2)M_d^2(1 + k^2c^2/\omega_{pe}^2)\}^{1/2}$$

This is equivalent to the corresponding result of Papadopoulos *et al.* (1971) only in the limit $k^2c^2 \gg \omega_{pe}^2$. The mode with maximum growth is then found from $d\omega/dk = 0$.

III. Shock Structure and Discussion

To examine the implications of this magnetosonic instability for collisionless shock structure, a shock layer is modeled as a region of interpenetrating upstream (unshocked) and downstream (shocked) ions (*e.g.*, Golden *et al.* 1973). In the reference frame of the leading edge of the shock the ion velocity distribution takes on the bimodal Mott-Smith form

$$f_i(x, V) = n_u(x)\delta(V - V_u) + n_d(x)\delta(V - V_d)$$

and for the electrons

$$f_e(x, V) = n_e(x)\delta(V - V_e(x))$$

In these distributions V_u and V_d are the average

upstream and downstream ion velocities and $n_u(x)$ and $n_d(x)$ are the respective ion densities through the shock. The corresponding electron quantities are determined by the charge and current neutrality conditions as

$$n_e(x) = n_u(x) + n_d(x)$$
$$V_e(x) = [1 - \eta(x)]V_u + \eta(x)V_d$$

where $\eta(x) = n_d(x)/n_e(x)$.

The results of the preceding section may now be applied to the shock structure problem by Doppler shifting the frequency ω according to $\omega = \omega_s - kV_e$ and using the Rankine–Hugoniot relations for a magnetic shockwave. The growth rate of the weak beam theory may be used to examine the behavior of unstable modes in the leading edge of the shock. If this instability is to play a role in structuring a weak collisionless shock, then unstable modes should either have zero group velocity in the frame of the leading edge or should propagate slowly downstream. Although the modes are found to propagate into shock, even the maximum growth rates are sufficiently small that the modes must travel an appreciable fraction of the shock thickness before experiencing an e fold increase in amplitude. A typical calculation of the e folding distance $\Delta = \gamma^{-1}d\omega_s/dk$ for the maximum growth mode near the leading edge of an air plasma shock shows that $\Delta = 7.3c/\omega_{peo}$ (subscript 'o' refers to leading edge conditions) for an upstream Alfvén Mach number $M_A = 2^{1/2}$ and $\gamma_g = c_p/c_v = 2$. In this case a choice of $\eta = (m_e/m_i)^{1/2}$ is simultaneously small enough to insure validity of the perturbation expansion yet not too small to violate the last of inequalities [2]. Since the shock thickness $L_s \sim 12c/\omega_{peo}$ (Golden *et al.* 1961), it is unlikely that this leading edge mode contributes to the structure of the shock.

It is also useful to consider the e folding growth distances for unstable modes generated in and propagating into the midshock region ($\eta = 1/2$). In the frame of the shock leading edge it is found from [4] that $d\omega_s/dk = V_u$ so that $\Delta = \gamma^{-1}(k)V_u$.

In particular for an air plasma shock of $M_A = 2^{1/2}$ and $\gamma_g = 2$ two typical conclusions may be reached: (*i*) for the leading edge mode of maximum growth, assumed to reach the shock midpoint while still in the linear stage, the e folding length is reduced only to $4.4c/\omega_{peo}$ so that the variation of Δ through the shock is not sufficiently strong to achieve much shorter e folding lengths, and (*ii*) the maximum growth mode at $\eta = 1/2$ produces a minimum Δ of $3.6(c/\omega_{peo})$ so that even this mode can only grow $1\frac{1}{2}$–2 e folds as it propagates from the midshock region to the trailing edge. It should be noted that these results are typical and relatively insensitive to the choice of γ_g and to the shock strength.

IV. Conclusions

The results of this study have been a complete analysis of the magnetosonic two stream instability including growth rates, limits of validity, and unstable spectra for both the weak beam–magnetosonic mode interaction and the equidense counterstreaming beam instability. Further, it has been found that this instability is probably not an important source of turbulent dissipation for the structure of weak shocks. On the other hand, for shocks where the initial steepening is broadened by classical dissipation, the instability might play a role in broadening the trailing edge. As a consequence it is now believed that perpendicular, collisionless shocks are structured by turbulence originating from the so called current driven modified two stream instability (Ott *et al.* 1972).

GOLDEN, K. I., LINSON, L. M., and MANI, S. A. 1973. Phys. Fluids, **16**, 2319.

GOLDEN, K. I., SEN, H. K., and TRÉVE, Y. M. 1961. *In* Proceedings of the Fifth International Conference on Ionization Phenomena in Gases (North Holland, Amsterdam), p. 2109.

OTT, E., MCBRIDE, J. B., ORENS, J. H., and BORIS, J. P. 1972. Phys. Rev. Lett. **28**, 88.

PAPADOPOULOS, K., DAVIDSON, R. C., DAWSON, J. M., HABER, I., HAMMER, D. A., KRALL, N. A., and SHANNY, R. 1971. Phys. Fluids, **14**, 849.

APPENDIX B

The attached Physics Letter reprint summarizes some initial aspects of our research on the application of streaming plasma instabilities to parallel shock wave structures. A complete discussion of this work is given in Sec. B of this report.

ROLE OF STREAMING PLASMA INSTABILITIES IN PARALLEL SHOCK WAVE STRUCTURES

J.W. CIPOLLA* and K.I. GOLDEN**
Department of Mechanical and Electrical** Engineering, Northeastern University, Boston, Massachusetts 02115, U.S.A.*

Received 5 February 1975

A parallel shock structure is modeled as regions of interpenetrating streams of cold unshocked ions and hot shocked ions. Our linear dispersion theory predicts that unstable whistlers can stand at the leading edge of weak and intermediate strength shocks.

Recently [1], it was proposed that unstable beam-whistler wave interactions formed the turbulent structure of shock waves propagating along the magnetic field (parallel shocks) in collisionless plasmas. It was assumed that the electrons could be modeled as warm fluid and the ions as a Mott Smith superposition of the unshocked and shocked ion flows: for mathematical simplicity, these ion flows were modeled as cold monoergetic beams. Analysis of the ensuing linear dispersion relation then revealed the existence of unstable modes standing near the leading edge of the shock for Alfvén Mach numbers $M_A \geqslant 5.5$. This suggests that such modes are most likely to grow to sufficiently large amplitude to scatter incoming ions and create the required dissipation for intermediate strength shocks. It was recognized, however, that the assumption of cold ion streams was a serious limitation in the theory since (i) the shocked downstream ions are, in any case, thermalized, and (ii) the upstream ions must be sufficiently warm ($C_s = \sqrt{\gamma\kappa(T_e + T_i)/m_i} > C_A = B_o/\sqrt{4\pi\rho_u}$; B_o = constant magnetic field, ρ_u = upstream mass density) to preclude the possibility of "switch-on" shocks (rotation of the magnetic field across the shock layer).

In this letter, we partially relax the cold ion stream requirement of the previous theory by more realistically allowing the downstream ions to be Maxwellian with final temperature T_d and mean velocity V_d dictated by the Rankine-Hugoniot relation. Then following the the Mott-Smith formalism, the ions, in the rest frame of the shock front, are modeled as the superposition of two streams: hot downstream particles moving with relative velocity $(V_d - V_u)$ through the cold upstream particles. The appropriate velocity distribution function for the ions at the station z inside the shock is therefore given by

$$f_i(z, v) = n_u(z)\,\delta(v - V_u) + \frac{n_d(z)}{\pi^{3/2} C_d^3} \exp\left[-\frac{(v - V_d)^2}{C_d^2}\right], \tag{1}$$

where $C_d = \sqrt{2\kappa T_d/m_i}$. The warm background electrons move with mean velocity $V_e(z) = [1 - \eta(z)]\,V_d + \eta(z) V_c$, $(\eta = n_d/(n_u + n_d))$, dictated by the requirements of local charge and current neutrality. Only weak beam-plasma interactions ($\eta \ll 1$) are considered here (applicable therefore to the leading edge of the shock layer) and considerations of arbitrary hot beam strengths are deferred to a later paper.

For the case of parallel propagation ($k \| B_o \| z$-axis), the linear dispersion relation is, in the electron rest frame,

$$\epsilon_{xx}(k\omega) \pm i\epsilon_{xy}(k\omega) = (kc/\omega)^2 . \tag{2}$$

The dielectric components in (2) are calculated by addition of the ion and electron polarizabilities. These well-known polarizabilities are formulated explicitly in terms of the (unperturbed) ion and electron distribution functions and therefore take account of the bimodal nature of the ions (eq. (1) in the shock reference frame) and the locally Maxwellian behavior of the electrons. We make the following low frequency approximations: (i) the vacuum displacement current is negligibly small ($\omega \ll kc$); (ii) the electrons have zero mass ($|\omega| \ll \Omega_{ce} = eB_o/m_e c$) so that they can be modeled as warm fluid ($kr_{Le} \ll 1$). The dispersion relation in the reference frame of the shock front

then ultimately becomes

$$[1-\eta(z)]\frac{\Omega_{ci}}{\omega_s - kV_u + \Omega_{ci}} + \eta(z)\frac{\Omega_{ci}}{\sqrt{\pi}C_d}\int_{-\infty}^{\infty}\frac{du\exp[-(u/C_d)^2]}{(\omega_s - kV_d + \Omega_{ci}) - ku} = 1 + \frac{k^2C_A^2(z)}{\Omega_{ci}^2} - \frac{\omega_s}{\Omega_{ci}} - \frac{kV_e(z)}{\Omega_{ci}}, \tag{3}$$

where $\omega_s = \omega + \boldsymbol{k}\cdot\boldsymbol{V}_e$ is the frequency in the shock frame. Note that the cold dispersion relation (5) of ref. [1] is recovered from (3) by letting $C_d \to 0$ and transforming back to the electron frame. The solution of eq. (3), $\omega_s = \omega_s(k)$, should provide the spectrum of unstable growth modes. Only those growth modes which have zero group velocity (in the shock front rest frame) are of interest, since only these have sufficient time to grow to large amplitude to scatter incoming particles.

In the weak beam ($\eta \ll 1$) approximation, we set $\omega_s = \nu + i\gamma$, $\gamma \ll |\nu|$. The solution of (3) is then readily found to be:

$$\nu(k; V_u) = kV_u + k^2C_A^2/(2\Omega_{ci}) - kC_A\sqrt{1+(kC_A/2\Omega_{ci})^2}\,, \tag{4}$$

$$\frac{\gamma(k; V_u)}{\Omega_{ci}} = \frac{\sqrt{\pi}\,\Omega_{ci}}{|k|C_d}\eta\frac{(\nu - kV_u + \Omega_{ci})^2}{(\nu - kV_u)(\nu - kV_u + 2\Omega_{ci})}\exp\left[-\frac{(\nu - kV_d + \Omega_{ci})^2}{k^2C_d^2}\right]. \tag{5}$$

Strong interaction evidently corresponds to the intersection of the $\nu - kV_d + \Omega_{ci} = 0$ hot ion beam line with the cold whistler dispersion curve, eq. (4), in the third quadrant of the (ω_s, k)-plane. Here the resulting γ_{max} varies directly with the strength η of the hot beam. In the previous theory [1], where the shocked ions were modeled as a cold monoenergetic beam, the corresponding weak ion beam-whistler interaction was found to be stronger, i.e. $\gamma_{max} \propto \sqrt{\eta}$. This is not surprising since, in the present theory, the whistler wave interacts strongly only with a small percentage of the hot beam ions, whereas in the previous theory, *all* of the particles in the monoenergetic ion beam participate in the interaction.

The ($\eta \ll 1$) zero group velocity condition $\partial\nu(k, V_u)/\partial k = 0$, readily obtained from (4), reveals that a given shock velocity $V_u \geq C_A$ corresponds to a given value of $k \leq 0$. From (4) and (5) we see that $k < 0$ is sufficient for $\gamma(k) > 0$, so that whistlers standing at the leading edge grow there (this instability does not, for the most part, correspond to an intersection between the hot ion beam line and the whistler dispersion curve) This is evidently true for all $M_A \geq 1$ up to the limit of validity of our $m_e = 0$ model (given by $M_A \leq (2/3)\sqrt{m_i/m_e}$, see ref. [1]). Thus the turbulent whistler mode structure for intermediate shocks ($M_A \geq 5.5$) suggested by the previous cold beam theory is suggested as well for weak shocks ($1 \leq M_A \leq 5.5$) by the present hot beam theory.

This work was supported by the U.S. Air Force under Contract No. F19628-75-C-0012.

Reference

[1] K.I. Golden, L.M. Linson and S.A. Mani, Phys. Fluids 16 (1973) 2319.

ERRATA

J.W. Cipolla and K.I. Golden, Role of streaming plasma instabilities in parallel shock wave structures, Physics Letters 51A(1975)251.

Equation (3) should be modified to read:

$$[1 - \eta(z)] \frac{\Omega_{ci}}{\omega_s - kV_u + \Omega_{ci}} + \eta(z) \frac{1}{\sqrt{\pi}\, C_d} \int_{-\infty}^{\infty} du \exp\left[-(u/C_d)^2\right] \frac{\Omega_{ci} - ku}{(\omega_s - kV_d + \Omega_{ci}) - ku} =$$

$$= 1 + \frac{k^2 C_A^2(z)}{\Omega_{ci}^2} - \frac{\omega_s}{\Omega_{ci}} + \frac{kV_e(z)}{\Omega_{ci}} .$$

Equation (5) should be modified to read:

$$\frac{\gamma(\underset{\sim}{k};V_u)}{\Omega_{ci}} \approx \frac{\sqrt{\pi}}{|k| C_d} \eta \frac{(\nu - kV_u + \Omega_{ci})^2 (kV_d - \nu)}{(\nu - kV_u)(\nu - kV_u + 2\Omega_{ci})} \exp\left[- \frac{(\nu - kV_d + \Omega_{ci})^2}{k^2 C_d^2} \right] .$$

Page 252, last paragraph, on lines 2 and 3 instead of "From (4) and (5), we see that $k < 0$ is sufficient for $\gamma(k) > 0$, so that whistlers standing..." should be written "From (5), we see that $\nu(k;V_u)/V_d < k < 0$ is sufficient for $\gamma(k) > 0$, so that certain whistlers standing ...."

Page 252, last paragraph, on line 5 instead of $M_A \geq 1$ should be written $M_A \geq 2.76$.

Page 252, last paragraph, second line from bottom, instead of $1 \leq M_A \leq 5.5$ should be written $2.76 \leq M_A \leq 5.5$.

These modifications do not alter the main statement of our paper.